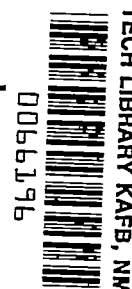


9393

NACA TN 3093



NATIONAL ADVISORY COMMITTEE FOR AERONAUTICS

TECHNICAL NOTE 3093

EFFECT OF TYPE OF POROUS SURFACE AND SUCTION VELOCITY
DISTRIBUTION ON THE CHARACTERISTICS OF
A 10.5-PERCENT-THICK AIRFOIL
WITH AREA SUCTION

By Robert E. Dannenberg and James A. Weiberg

Ames Aeronautical Laboratory
Moffett Field, Calif.



Washington
December 1953

AFMEC
TECHNICAL LIBRARY
AFL 2611

Y



TECHNICAL NOTE 3093

EFFECT OF TYPE OF POROUS SURFACE AND SUCTION VELOCITY
DISTRIBUTION ON THE CHARACTERISTICS OF
A 10.5-PERCENT-THICK AIRFOIL
WITH AREA SUCTION

By Robert E. Dannenberg and James A. Weiberg

SUMMARY

An investigation has been made at low speed of the two-dimensional characteristics of a 10.51-percent-thick symmetrical airfoil with area suction for boundary-layer control near the leading edge. The lift and suction-flow characteristics were determined with different porous surfaces consisting of perforated plates and sintered steel for various suction velocity distributions obtained by varying the permeability arrangement. The flow requirements were ascertained over a range of free-stream velocities.

The maximum section lift coefficient was increased from 1.3 to approximately 1.8 by means of area suction from 0.3- to 3.0-percent chord. For the airfoil investigated, a lift coefficient of 1.7 was attained with a minimum section flow coefficient of 0.00090 at a free-stream velocity of 162 feet per second with a permeability arrangement which gave a suction velocity at the trailing edge of the suction area equal to 2 percent of the local velocity with no outflow at the leading edge.

The maximum lift coefficient and the minimum suction quantity for a given lift were independent of the surface of the materials tested (including filter paper, NACA TN 2847). The minimum flow coefficient required for a given increase in lift varied with free-stream velocity; the amount depended on the chordwise distribution of the porous material.

INTRODUCTION

The maximum lift of moderately thick wing sections (9 to 12 percent of the chord) is generally limited by separation of the flow near the wing leading edge. It has been demonstrated that leading-edge flow separation may be prevented with boundary-layer control by means of suction through suitable slots or through a porous area at the leading edge of the wing.

An investigation of the latter method is reported in reference 1. The airfoil had a 10.51-percent-thick symmetrical section. The maximum lift of this airfoil, without boundary-layer control, was limited by leading-edge type of stall. Boundary-layer suction through a porous region in the upper surface near the leading edge proved to be effective in delaying separation of flow from the leading edge and in postponing the stall to higher angles of attack. The stall of the airfoil with suction appeared to result from separation of the turbulent boundary layer from the trailing edge. Filter paper backed by a metal screen was used as the porous material.

In order to ascertain: (1) the effect of surfaces of different textures, (2) the effect of variations of chordwise distribution of suction velocity, and (3) the effect of free-stream velocity on maximum lift and on the minimum suction quantity for a given lift, a second investigation - the subject of this report - was made. The 10.51-percent-thick symmetrical airfoil of reference 1 was modified to accommodate detachable perforated metal plates and sintered-steel nose sections. The tests included measurements of the surface pressure distributions, profile drag, suction flow, and the boundary layer. The investigation was conducted in one of the Ames 7- by 10-foot wind tunnels.

NOTATION

- c airfoil chord, ft
- c_{d_0} section-profile drag coefficient, $\frac{D}{q_0 c}$, as determined from wake surveys
- c_l section lift coefficient, $\frac{L}{q_0 c}$, as determined from integration of the chordwise distributions of pressure
- c_m section pitching-moment coefficient referred to the quarter-chord point, $\frac{M}{q_0 c^2}$, as determined from integration of the chordwise distribution of pressure
- c_Q section flow coefficient, $\frac{\int v ds}{c U_0}$
(The limits of integration are the foremost and rearmost chordwise points of area suction.)
- c_w suction power coefficient (ref. 1),

$$\frac{1}{c q_0 U_0} \left(\frac{\gamma}{\gamma-1} \right) Q_1 p_1 \left[\left(\frac{p_0}{p_1} \right)^{\frac{\gamma-1}{\gamma}} - 1 \right]$$

- D drag per unit span, lb
- H boundary-layer-shape parameter $\frac{\delta^*}{\theta}$
- Δh total-pressure loss, in. of water
- L lift per unit span, lb
- M pitching moment per unit span, referred to the quarter-chord point, lb-ft
- P pressure coefficient, $\frac{P-P_0}{q_0}$
- p static pressure, lb/sq ft
- Q volume rate of flow per unit span, cu ft/sec
- q_0 free-stream dynamic pressure, $\frac{1}{2}\rho_0 U_0^2$, lb/sq ft
- s distance along airfoil surface, ft
- U local velocity outside boundary layer, fps
- U_0 free-stream velocity, fps
- u local velocity within boundary layer, fps
- v suction air velocity normal to outer surface of the airfoil, fps
- x distance from airfoil leading edge measured parallel to chord line, ft
- y distance from airfoil measured normal to surface, ft
- α angle of attack, deg
- γ ratio of specific heats for air, taken as 1.4
- δ total boundary-layer thickness, ft
- δ^* boundary-layer displacement thickness, $\left[\int_0^\delta \left(1 - \frac{u}{U} \right) dy \right]$, ft
- θ boundary-layer momentum thickness, $\left[\int_0^\delta \frac{u}{U} \left(1 - \frac{u}{U} \right) dy \right]$, ft

- τ index of resistivity defined as the total-pressure difference in inches of water required to induce a suction air velocity of 1 fps through a porous material of a given thickness
- ρ mass density of air, slugs/cu ft

Subscripts

- e local external point
- o free-stream conditions
- 1 conditions in suction duct
- u uncorrected
- 0.6 }
2.9 } station, percent chord
3.0 }

MODEL AND APPARATUS

Model

A 4.5-foot-chord, two-dimensional model was used for this investigation and is shown in figure 1. Coordinates of this 10.51-percent-thick symmetrical section are given in table I, together with a sketch comparing the profile with a symmetrical NACA 4-digit 00-series airfoil of equal maximum thickness. Flush orifices in the outer surface of the model permitted measurement of the pressure distribution.

The end-plate and slat arrangement shown in figure 1 was used to minimize the effects of the tunnel-wall boundary layer and is described in reference 1. The span between the end plates was 5 feet.

The model contained an internal plenum chamber and ducting for the porous nose as described in reference 1. The details of the model construction are shown in figure 2. Flush orifices were used to measure the internal static pressures. The cross-section area of the plenum chamber and ducting was large enough to reduce the dynamic pressure of the induced air to negligible values and to insure uniform internal pressures across the span of the model.

The porous leading-edge portion of the model was removable to facilitate model changes. The external surface of the porous nose sections consisted of a porous metal sheet, spot welded to 1/16-inch-thick ribs spaced approximately 4.6 inches. The external metal sheet extended from approximately 7-percent chord on the upper surface around the nose to approximately

4-percent chord on the lower surface. The different types of external surface materials used are shown in figure 3. These materials are described in table II.

Material 1 was an electroplated metal screen. Materials 2, 3, and 4 were perforated metal plates. Material 5 was a porous, sintered, stainless steel. The metal surfaces were backed with a permeable material which consisted of a commercial grade of felt or a combination of felt and filter paper. The felt was held against the surface material by a 12-mesh, 0.025-inch-diameter wire cloth supported by 1/8-inch-diameter rods which passed through the metal ribs as shown in figure 2. For the felt and filter-paper combinations, the filter paper was inserted between the felt and the outer metal surface.

With the different outer surfaces, several arrangements of felt thickness variation and several combinations of felt and filter paper were used to obtain various suction velocity distributions. The various permeability arrangements tested are described in table III. The chordwise variations of the index of resistivity for these arrangements are given in table IV. The flow resistances of several of the porous materials are given in figure 4. The data in figure 4(a) for perforated plate 1 with felt backing are typical of all the perforated plates with felt backing.

The tests were made with various chordwise extents of porous area obtained by closing off portions of the porous surface with a nonporous tape between the felt and the outer metal surface.

Apparatus

The suction pressure required to induce flow through the porous material was provided by a variable-speed compressor located outside the wind tunnel. Air was drawn through the porous nose into the hollow spar in the airfoil and then through the ducting system to the compressor.

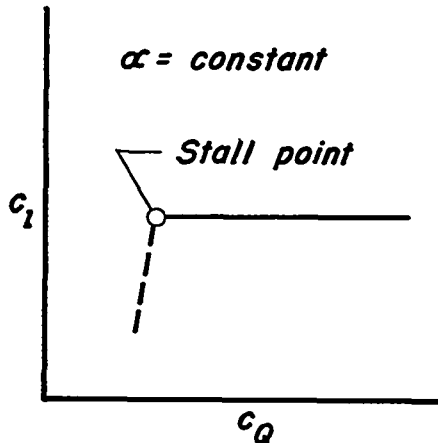
Boundary-layer measurements were made with a small pressure rake attached to the surface of the model. Aural observations of the boundary layer were made with a stethoscope. A survey rake connected to an integrating manometer was used to measure rake pressures for the calculation of wake drag.

TEST METHODS

Air flow through the porous area of the airfoil was induced by maintaining a pressure inside the model that, generally, was less than the external pressure. The suction air velocity at a given chordwise station was calculated from the measured pressure difference across the porous material and from the known flow resistance of the porous materials. The flow-resistance characteristics of the surface materials with various arrangements of felt thickness and of felt and filter paper were ascertained experimentally by the method described in reference 1. The section

flow coefficients c_Q were calculated from integration of the suction velocity distributions.

Previous tests of the model with a porous leading edge, reported in reference 1, have indicated that for angles of attack near that for maximum lift (15° or greater), there is a value of section flow coefficient



c_Q below which the model stalls abruptly, as indicated in the adjacent sketch. For lower angles of attack the stall was not as abrupt. The c_Q at a given angle of attack for which the large change in lift occurs will hereafter be designated as the stall point c_Q . In order to obtain close agreement between the different arrangements it was necessary to ascertain the stall point as accurately as possible. The method of ascertaining the stall point was to maintain constant angle of attack as the section flow coefficient was decreased from the maximum until the model stalled. To determine if the unstalled lift at a given angle of attack could be regained after the c_Q

had been reduced below its stall point, data were obtained as the c_Q was increased without changing the angle of attack. The results showed that for angles of attack at which an abrupt loss in lift occurred at the stall point ($\alpha = 15^\circ$ and above), the model could not be unstalled once the c_Q had been reduced below the stall-point value by increasing the c_Q to the maximum obtainable with the suction pump. For angles of attack of 14° and below, the model could be unstalled by increasing the suction quantity to the stall-point value. The stall points were repeatable to within a c_Q of 0.0003 (0.3- to 3-percent chordwise extent of suction).

The tests covered a range of free-stream velocities from 66 (Mach number 0.05) to 187 feet per second (Mach number 0.17). The corresponding Reynolds numbers, based on the airfoil chord, were 1.8 to 5.1 million, respectively. Wake drag data were obtained at a Reynolds number of 5.1 million.

The lift was evaluated from measurements of a manometer which integrated the surface pressure distribution. The profile drag was calculated from wake pressures measured by a rake one-half chord length behind the trailing edge of the airfoil. Moments were evaluated from pressure-distribution diagrams.

Tunnel-wall corrections have not been applied to the data. The angle correction in degrees normally added to the angle of attack for correcting the data to free-air conditions, as described in reference 2, is 0.384 times the section lift coefficient.

At the start and during the investigation of each permeability arrangement, calibrations were made (1) to check the quantity flow rates — particularly with a tapered felt backing material — and (2) to determine the effect of dust, etc., in the suction air on the flow resistance of the permeable material.

The flow resistances of the permeable nose sections on the model were determined from measurements made with a standard A.S.M.E. orifice in the suction line between the model and the compressor. At the start of the tests, measurements of the flow rates through the permeable nose sections for the various permeability arrangements, both with tunnel off and with air flow past the model, showed agreement between the values measured with the orifice and the values obtained from the integrated suction velocity diagrams.

The permeability arrangements consisting of the perforated-plate nose sections backed with felt showed no tendency to clog over long periods of operation. For example, permeability arrangement A was in operation over 100 hours; arrangement B, 24 hours; arrangement C, 175 hours. The accumulation of dust from the suction air during the testing discolored the felt surface nearest the outer surface material but the discoloration did not penetrate more than 1/16 inch into the felt. Flow-resistance calibrations made at the start and at the completion of testing were identical.

With the sintered-steel nose section, a change in the flow resistance was noted after 22 hours of operation. To determine the clogging effects, the backing material was removed for each calibration. The variation with time of operation of the flow resistance of the sintered-steel nose without backing is shown in figure 5. The data indicate approximately 25-percent reduction in suction velocity at a given pressure drop for a 68-hour period. At the end of this period, the nose section was removed from the model and a high-pressure air flow (25 psi) was blown through the nose in a reverse direction for several minutes. In addition, the nose was washed with gaseous trichloride ethylene. The cleaning did not appreciably change the flow resistance. Over the total period of operation, the suction velocities for a given pressure drop were reduced approximately 50 percent.

The data presented for the sintered-steel nose section (arrangements K and L) were obtained in the first 22 hours of operation. Data obtained after this time have not been presented, except for the calibration curves shown in figure 5, as clogging resulted in a measurable change in the stall points.

RESULTS AND DISCUSSION

Plain Airfoil

Evaluation of area suction as a means of boundary-layer control can be made by comparison of the results for the plain airfoil with those for the airfoil with area suction. The lift, profile-drag, and pitching-moment coefficients of the plain airfoil from reference 1 are given in figure 6. The data in figure 6 indicate that the maximum lift of the airfoil was limited by leading-edge stall (ref. 3). This type of stall is

characterized by abrupt changes in the lift and pitching moment, with little or no rounding-over of the lift curve near maximum lift, when the angle of attack for maximum lift is exceeded. The increase in profile drag with lift is moderate up to the stall. The chordwise distributions of pressure in figure 7 show an increase in the peak negative pressures up to the stall, followed by an abrupt collapse with redistribution of the pressures giving the flat-type pressure-distribution characteristic of separated flow. This redistribution of pressure after the stall results in a rearward shift in the center of pressure and the abrupt decrease in pitching moment shown in figure 6.

Airfoil With Various Chordwise Extents of Area Suction
(Constant Free-Stream Velocity of 162 fps)

The determination of the optimum chordwise extent of suction for maximum lift was made by using the airfoil with the nose porous from 3-percent chord on the lower surface to 5-percent chord on the upper surface and by progressively closing off various portions of the porous surface with a nonporous tape. The results for external surface material 1 (table II) and uniform permeability arrangement A (table III) are shown in figure 8 for suction flow coefficients above the stall-point value.

Figure 8 shows that reducing the chordwise extent of area suction to less than from 0.3- to 3-percent chord resulted in a decrease in maximum lift. With suction over more than from 0.3- to 3-percent chord, the value of the maximum lift was not changed significantly but the quantity of suction flow was increased, particularly by the use of suction on the lower surface. Similar results were shown by the data presented in reference 1.

Reducing the chordwise extent of area suction from the maximum investigated (3-percent-chord lower to 5-percent-chord upper surface), for all practical purposes, did not change the magnitudes of the suction velocities for the stall points.

The optimum chordwise extent of suction for maximum lift was determined for other surface materials and permeability arrangements and also was found to extend from 0.3- to 3-percent chord on the upper surface. Therefore, the remainder of the data presented for a free-stream velocity of 162 feet per second are for the airfoil with this chordwise opening.

As will be shown later in the discussion, the optimum chordwise opening varied with free-stream velocity.

Effect of External Surface and Permeability Arrangement
(Constant Free-Stream Velocity)

With the nose porous from 0.3- to 3-percent chord, the suction flow quantity to obtain a given lift with various surface materials and permeability arrangements was determined. The permeability arrangements tested are given in table III. Permeability arrangements A and B had a constant thickness of felt backing material over the porous area. For arrangements C, D, E, K, and L the thickness of backing material increased from the leading edge of the suction area to the trailing edge. These arrangements of backing material in combination with the various surface materials resulted in a smooth chordwise variation of the suction velocities. Arrangements F through J were arrangements A, B, and C, combined with filter paper inserted between the felt cloth and the outer metal surface. As the filter paper extended over only the rearward portion of the porous area, an abrupt increase in the resistivity occurred where the filter paper started and resulted in stepped variations of the suction velocity.

The variables involved in a discussion of the results in terms of external aerodynamic coefficients are many. They include surface condition, suction velocity distribution, and free-stream velocity. The first part of the discussion is concerned with the effects of surface condition and suction velocity distribution at a given free-stream velocity. Later in the discussion the effects of free-stream velocity on these variables are considered.

Lift characteristics.— Representative lift and flow characteristics of the model with a porous leading edge are shown in figure 9 for suction-off and suction-applied conditions. Data are presented for two suction-off conditions obtained by (1) closing the suction air line between the model and the suction pump — in this condition some air flowed through the porous area, generally with outflow over the forward portion and inflow over the rearward portion, and by (2) sealing the porous surface with a nonporous tape between the porous metal surface and the felt backing — the outer surface of the porous material remained unchanged.

The data in figure 9 are for the model with surface material 1 and permeability arrangement C (0.3- to 3-percent chordwise extent of suction). For angles of attack of 14° or less (c_l less than about 1.5) these data are typical of the data for all surface materials and permeability arrangements tested. For angles of attack greater than 14° , the values of the lift and of the stall point c_{q_s} were a function of the particular permeability arrangement, as shown in parts (a) and (b) of the figures listed in the following table:

Figure	Surface material (table II)	Permeability (table III)
10	Perforated plate 1 and [2,3,4]	A
11	— do — 1 and [3]	B
12	— do — 1 and [2]	C
13	— do — 1	D
14	— do — 1	E
15	— do — 1	F
16	— do — 2 and [1]	G
17	— do — 2	H
18	— do — 2	I
19	— do — 2	J
20	Sintered steel	K
21	— do —	L

Data were also obtained with the outer surface materials listed in the brackets in the above table but are not presented. These data were, for all practical purposes, the same as those presented.

A study of the lift characteristics of the model in parts (a) of figures 10 through 21 indicates that a maximum lift coefficient from 1.72 to 1.80 was attained at an angle of attack of 17° . The slight differences in the values of the maximum lift coefficient are not considered significant in regard to effects due to surface materials or permeability arrangements. The lift coefficient of 1.70 obtained at an angle of attack of 17° with permeability arrangement J (fig. 19) appeared to be limited by the suction power available.

The stall-point section flow coefficient and the maximum lift coefficient of the airfoil used in this investigation, for practical purposes, were independent of the roughness of the external surface material; that is, filter paper, perforated plate, or sintered steel gave essentially equal maximum lift. The maximum lift was independent of the arrangement of the permeability; however, the section flow coefficient necessary for maximum lift was dependent on the suction velocity distribution.

Suction velocity distribution.— Because it was difficult to obtain consistent data at the angle of attack for maximum lift coefficient of the airfoil ($\alpha \approx 17^\circ$), the flow characteristics are compared at a lower angle of attack. The suction velocity distributions for various section flow coefficients are shown in part (c) of figures 10 through 21 for an angle of attack of 16° . The velocity distribution for the least value of c_Q represents that for the stall point. The corresponding values of plenum-chamber pressure coefficient are tabulated in table V. The maximum values of c_Q for angles of attack of 16° and 17° shown in part (a) of figures 10 through 21 are the maximum values obtainable with the suction pump. A comparison of the stall-point suction velocity distribution for an angle of attack of 16° for the various smooth-type permeability arrangements tested is shown in figure 22. The section flow and

section lift coefficients and plenum-chamber pressure coefficients for the stall points are tabulated in the figure. Included in figure 22 is the stall-point suction velocity distribution for the arrangement with a filter-paper surface (configuration A of ref. 1).

At the stall point for arrangements A and L, the suction velocities at the leading edge of the suction area ($x/c = 0.003$) were approximately zero. For the other permeability arrangements (including arrangement L), the suction velocities at the trailing edge of the suction area ($x/c = 0.03$) were about 7 feet per second ($(v/U)_{3.0} = 0.0170$). Thus, it appears that, for the airfoil investigated, the optimum smooth-type permeability arrangement to obtain maximum lift with minimum section flow coefficient at an angle of attack of 16° and a free-stream velocity of 162 feet per second is one designed for a suction velocity at the trailing edge of the suction area of the order of 7 feet per second with no outflow at the leading edge of the suction area.

The variation of the stall-point suction velocity at the trailing edge of the suction area with section lift coefficient is shown in figure 23 for some of the smooth-type permeability arrangements. Data for which the stall point was limited by outflow near the leading edge were not included. For the arrangements shown in figure 23, the maximum lift was attained with a value of suction velocity $v_{3.0}$ of approximately 2 percent of the local velocity outside the boundary layer at 3-percent chord. Increasing the value of $v_{3.0}$ to 5 percent of the local velocity did not increase the maximum lift. At maximum lift the local Mach number at the point of minimum pressure ($x/c = 0.0028$) was approximately 0.70, while at 3-percent chord the Mach number was approximately 0.39.

In figure 24(a) are presented the suction velocity diagrams for the stall point at an angle of attack of 16° for the various stepped distributions of permeability tested. Due to the high flow resistance of permeability arrangements F to J in the rear portions of the suction area, decreasing the plenum-chamber pressures greatly increased the suction velocities over the leading edge of the suction area with relatively slight increase in the suction velocity over the rear portion (fig. 24(b)). Low values of c_q at the stall point at 16° angle of attack were obtained for stepped arrangements F and G; however, the lift coefficients were lower than with the smooth-type permeability arrangements for which results are shown in figure 22.

External pressure distribution.— Typical chordwise distributions of the external pressure coefficients for the model with smooth- and stepped-type permeability arrangements are shown in figures 25 and 26, respectively. The data in figure 25 are for perforated plate 1 with permeability arrangement C, and the data in figure 26 are for perforated plate 2 with permeability arrangement J. These data are typical for all the external surface materials and permeability arrangements for section flow coefficients above the stall point at a given angle of attack below that for maximum lift. In figure 27, the variations of the pressure coefficient at 5.75-, 20-, and 95-percent chord with angle of attack for section

flow coefficients above the stall point are presented for the model with various external surface materials. Near maximum lift, the pressure coefficients at the leading edge differed by an amount dependent on the value of the section lift coefficient.

Boundary-layer measurements.— Boundary-layer measurements at 95 percent of the model chord for surface material 5 (sintered steel) with permeability arrangement K are presented in figure 28 in the form of the derived boundary-layer momentum thickness θ/c and shape parameter H . With suction, the shape parameter attained a value of approximately 2.4 at an angle of attack that was dependent on the value of the suction velocity. Increasing the suction velocity $v_{3.0}$ above the stall-point value at an angle of attack of 16° (approximately 7 fps) did not alter the value of the shape parameter. The values of the momentum thickness and of the shape parameter are shown in figure 29 for suction velocities ($v_{3.0}$) of 5 and 8 feet per second for the model with surface materials consisting of filter paper (from ref. 1), sintered steel (material 5), and perforated plates 1 and 2. Values of the section flow coefficient for a suction velocity ($v_{3.0}$) of 8 feet per second and permeability arrangements C, D, H, and L of figure 29 can be obtained from part (c) of figures 12, 13, 17, and 21, respectively. Comparison of these values shows that the boundary-layer parameters at 95-percent chord are more dependent on maintaining a suction velocity above the stall-point value ($v_{3.0}$) than on the suction quantity.

With a single total-pressure tube (0.026-in. diam., 0.005-in. wall thickness) on the surface of the model at the trailing edge of the suction area (0.03 chord), the boundary layer could not be detected for suction velocities above the stall-point value of $v_{3.0}$ for the model with sintered steel and permeability arrangements K and L. As the boundary layer at the trailing edge of the suction area was extremely thin, the boundary-layer parameters at 95-percent chord were primarily a function of the pressure gradient and surface from the trailing edge of the suction area to the trailing edge of the airfoil. This may explain the fact that increasing suction velocities above the critical did not increase the lift for a given angle of attack nor did it increase the maximum lift. As the suction velocities were reduced below the stall-point values, the total-pressure tube indicated a measurable boundary layer at 0.03 chord, and stethoscopic observations indicated that the boundary layer was turbulent.

Profile-drag characteristics.— The profile-drag measurements were made at a free-stream velocity of 187 feet per second. The profile-drag characteristics of the model with the various suction-area materials are shown in figure 30(a) for the suction-off condition with the porous surface sealed (described under Lift Characteristics). The data indicated that the addition of the porous surface resulted in an increase in the profile drag and a decrease in the maximum section lift coefficient from 1.30 to approximately 1.15. The profile-drag characteristics of the

model with sintered steel and permeability arrangement K are shown in figure 30(b) for the suction-off and suction-applied conditions.

The drag characteristics of the model with suction, as a function of the section flow coefficient, are shown in figure 31 for a metal-mesh and sintered-steel surface material. Similar results were shown in reference 1, (fig. 15(b)) with the porous surface consisting of filter paper. A comparison of the profile-drag characteristics of the model with suction for a metal mesh, sintered-steel, and filter-paper surface material is presented in figure 32. The data indicate that the suction velocity $v_{s.o}$ necessary to maintain the profile drag at a low value was essentially independent of the type of surface tested.

Effect of Free-Stream Velocity

Flow characteristics.— The foregoing discussion of the lift and flow characteristics has been limited to the data obtained for a free-stream velocity of 162 feet per second. Data were also obtained to determine the effects of varying the free-stream velocity from 66 to 187 feet per second on the stall-point suction velocity distribution at an angle of attack of 16° . The results are presented in figure 33 for various surface materials and permeability arrangements.

With decreasing free-stream velocity, the stall-point suction velocities and, hence, the pressure differences through the porous material decreased. The flow-resistance characteristics of the permeable materials (fig. 4) were such that, for these low pressure differences, the stall-point suction velocity distributions for the various permeability arrangements approached the same general shape (fig. 33).

For low values of free-stream velocity some outflow occurred in a region near the leading edge of the suction area (fig. 33) even for suction flow coefficients greater than that required at the stall point. It was found that, for these low values of free-stream velocity, the chordwise extent of the opening could be reduced from the normal 0.3- to 3-percent chord to include only the area over which inflow occurred without affecting the lift characteristics. This reduction of the chordwise extent of the opening did not change the magnitudes of the suction velocities for the stall points.

Stall-point section flow coefficients for the arrangements given in figure 33 were evaluated by integration of the suction velocity over the chordwise extent of the inflow. The stall-point c_Q increased with increasing free-stream velocity as shown in figure 34. The model with permeability arrangement L showed the least variation of stall-point c_Q with free-stream velocity. Arrangement L results in the minimum values of stall-point c_Q for the arrangements tested for free-stream velocities

greater than 130 feet per second. Below 130 feet per second, arrangement D gave the minimum value of stall-point c_Q .

The variation with free-stream velocity of the ratio of the stall-point suction velocity to the local velocity at the trailing edge of the suction area ($\alpha_u = 16^\circ$) is shown in figure 35. These data indicate an increase in the stall-point suction velocity $v_{3.0}$ with an increase in the free-stream velocity. The fact that the ratio of the stall-point suction velocities to the free-stream velocity and, hence, c_Q varied with free-stream velocity indicates that c_Q , in itself, is not a complete aerodynamic coefficient for expressing suction requirements in boundary-layer-control applications involving area suction at the leading edge of an airfoil. Over the Reynolds number range of the tests (1,800,000 to 5,100,000) the stall-point suction velocity $v_{3.0}$ needed to prevent flow separation appeared to be proportional to U_o^n with n somewhat greater than 2.

Suction-power considerations at an angle of attack of 16° .— The suction power corresponding to the stall-point suction velocity distributions in figure 33 in terms of horsepower per foot of span were computed from the relation:

$$HP = \frac{c_w q_o U_o c}{550} \quad (1)$$

where

$$c_w = -c_Q P_1 \left[1 - 0.6429 \left(\frac{P_1 q_o}{P_o} \right) + 0.4898 \left(\frac{P_1 q_o}{P_o} \right)^2 - 0.4023 \left(\frac{P_1 q_o}{P_o} \right)^3 \right] \quad (2)$$

The derivation of the suction-power coefficient c_w is given in reference 1. The results of the power calculations are presented in figure 36. For free-stream velocities up to approximately 130 feet per second, the suction powers were less than 0.5 horsepower per foot of span.

For free-stream velocities from 130 to 187 feet per second, the suction power for all arrangements increased at a rate dependent upon the permeability arrangement, with the rate of increase being greater than the U_o^3 which would be indicated from equation (1) if c_w were constant. The lowest suction powers as well as the least change of power with free-stream velocity were obtained for arrangement L. With this arrangement, the suction power was approximately proportional to U_o^6 (see logarithmic plot in fig. 36). With arrangements A and K the power also increased approximately in proportion to U_o^6 , while with arrangements J and D it increased more rapidly.

Several factors contributed to the rapid increase of suction power with increasing free-stream velocity:

(1) The stall-point suction velocity ratio at the trailing edge of the suction area $(v/U)_{3.0}$ necessary to prevent flow separation increased with free-stream velocity.

(2) Because of (1), the plenum-chamber pressure coefficients increased. This increase, for the arrangements tested, was approximately in proportion to U_0 .

(3) Because of (1) and (2), the suction velocities over the forward portion of the porous area increased, resulting in an increase in c_Q . The magnitude of the variation of c_Q was dependent on the permeability arrangement.

CONCLUDING REMARKS

The maximum lift coefficient of the symmetrical 10.51-percent-thick airfoil was increased from 1.3 to approximately 1.8 by means of area suction from 0.3- to 3-percent chord. The maximum lift with suction appeared to be limited by turbulent separation from the trailing edge of the airfoil and was independent of the surface of the porous material (perforated plate, sintered steel, or filter paper).

The maximum lift coefficient and the minimum suction quantity for a given lift were independent of the roughness of the different surface materials. For the airfoil investigated to obtain a lift coefficient of 1.7 with minimum section flow coefficient at a free-stream velocity U_0 of 162 feet per second required a suction velocity at the trailing edge of the suction area of the order of 2 percent of the local velocity with no outflow at the leading edge of the suction area. For the permeability arrangement giving this velocity distribution, the minimum section flow coefficient was 0.00118. The suction velocity at the trailing edge of the suction area needed to prevent flow separation at an angle of attack of 16° appeared to be proportional to U_0^n with n somewhat greater than 2.

The suction quantity and power for a given lift were found to vary with free-stream velocity. The magnitude of the variation depended on the permeability arrangement. The suction horsepower required for a lift coefficient of 1.7 was proportional to U_0^n where n was approximately 6 or greater for the different permeability arrangements tested.

Ames Aeronautical Laboratory
National Advisory Committee for Aeronautics
Moffett Field, Calif., Sept. 18, 1953

REFERENCES

1. Dammenberg, Robert E., and Weiberg, James A.: Section Characteristics of a 10.5-Percent-Thick Airfoil with Area Suction as Affected by Chordwise Distribution of Permeability. NACA TN 2847, 1952.
2. Allen, H. Julian, and Vincenti, Walter G.: Wall Interference in a Two-Dimensional-Flow Wind Tunnel, with Consideration of the Effect of Compressibility. NACA Rep. 782, 1944.
3. McCullough, George B., and Gault, Donald E.: Examples of Three Representative Types of Airfoil-Section Stall at Low Speed. NACA TN 2502, 1951.
4. Anon.: Lektromesh Specification Sheet, The C. O. Jelliff Mfg. Corp., Southport, Conn., 1949.
5. Anon.: Perforated Materials, General Catalog No. 62, The Harrington and King Perforating Co., Chicago, Ill., 1950.
6. Anon.: Properties of Aircraft Quality Porous Stainless Steel, Aircraft Porous Media, Inc., Glen Cove, N. Y., 1952.
7. Anon.: Data Sheet No. 5, The American Felt Co., Glenville, Conn., 1947.
8. Anon.: Filter Paper, The Eaton-Dikeman Co., Mount Holly Springs, Penn., 1950.

TABLE I.- SYMMETRICAL AIRFOIL USED IN THE INVESTIGATION
[Percent airfoil chord]

(a) Coordinates

Station	Ordinate	Station	Ordinate
0	0	40	5.253
.5	1.08	45	5.164
.75	1.31	50	4.994
1.25	1.64	55	4.733
2.5	2.21	60	4.401
5	2.94	65	3.982
7.5	3.433	70	3.481
10	3.807	75	2.910
15	4.352	80	2.329
20	4.724	85	1.747
25	4.995	90	1.166
30	5.166	95	.583
35	5.255	100	0
L. E. radius: 1.304			

(b) Comparison with NACA 0010.51 airfoil

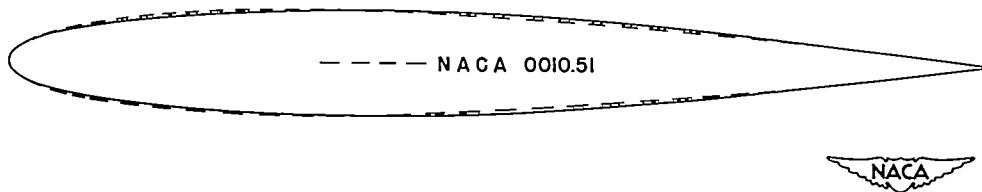


TABLE II.— CHARACTERISTICS OF THE MATERIALS USED
IN THE POROUS LEADING EDGE

No.	Material description				Refer- ence	Nom- inal thick- ness, in.	τ
Perforated plates							
		Hole size, in.	Holes per sq in.	Percent open			
1	65 count	0.005	4,225	10.5	4	0.006	0.018
2	No. 00 straight	.020	952	30.0	5	.016	.006
3	No. 4 straight	.050	169	33.0	5	.016	.004
4	No. 1/20 stag- gered	.050	57	11.2	5	.016	.019
Sintered steel							
5	Grade E				6	0.032	0.33
Felt							
	Color	lb/yd					
6	White	8.4			7	0.50	10.20
Filter paper (ref. 1)							
7	Grade 954, single sheet				8	0.0065	7.00
8	Grade 952, single sheet				8	.007	18.00


 NACA

TABLE III.— PERMEABILITY ARRANGEMENTS TESTED

Permeability arrangement	Felt thickness, in., at percent x/c of -				Surface material table II
	0.28	0.60	1.17	2.92	
Felt distributions used with perforated plates					
A	0.150	0.150	0.150	0.150	1,2,3,4
B	.508	.508	.508	.508	1,3
C	.125	.125	.250	.370	1,2
D	.062	.062	.210	.500	1
E	.035	.055	.140	.500	1
Filter paper and felt arrangements used with perforated plates					
F	Arrangement B (above) with material 8 (table II) from 1- to 3-percent chord				1
G	Arrangement A with material 8 from 1- to 3-percent chord				1,2
H	Arrangement A with material 7 from 1- to 3-percent chord				2
I	Arrangement A with material 8 from 2- to 3-percent chord				2
J	Arrangement C with material 7 from 1.5- to 3-percent chord				2
Felt distributions used with sintered steel					
K	0.062	0.106	0.202	0.317	5
L	.062	.134	.215	.215	5
Configuration A of reference 1					
M	Single sheet of material 7 (table II)				7

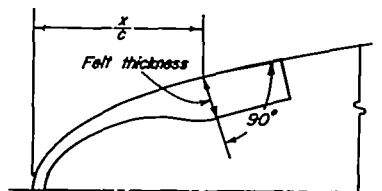
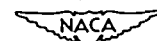


TABLE IV.— INDEX OF RESISTIVITY DISTRIBUTIONS FOR
THE PERMEABILITY ARRANGEMENTS TESTED

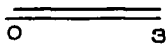
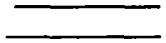
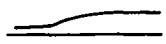
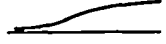
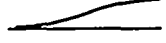



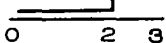
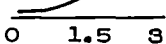


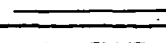
Permeability arrangement	Index of resistivity, τ , at percent x/c of —				τ against x/c , percent
	0.28	0.60	1.17	2.92	
A	3.50	3.50	3.50	3.50	
B	12.00	12.00	12.00	12.00	
C	3.00	3.00	6.00	8.90	
D	1.52	1.52	5.10	12.00	
E	.83	1.32	3.35	12.00	
F	12.00	12.00	37.00	37.00	
G	3.50	3.50	26.50	26.50	
H	3.50	3.50	10.20	10.20	
I	3.50	3.50	3.50	26.50	
J	3.00	3.00	6.00	15.00	
K	1.60	2.50	4.50	7.10	
L	1.60	3.10	4.80	4.80	
M	7.00	7.00	7.00	7.00	

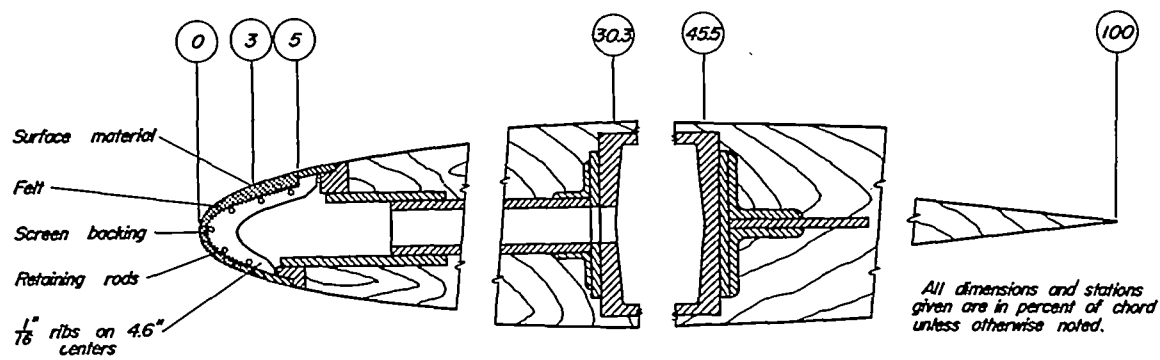
TABLE V.— PLENUM-CHAMBER PRESSURE COEFFICIENTS
 $[\alpha_u = 16^\circ]$

Figure	Surface material	Permeability arrangement	c_Q	P_1
10	1	A	0.00342	-25.5
			.00282	-22.6
			.00241	-20.7
			.00206	-19.7
11	1	B	.00166	-33.2
			.00138	-29.0
			.00108	-24.7
			.00286	-30.4
12	1	C	.00245	-28.1
			.00182	-23.7
			.00139	-20.8
			.00361	-30.4
13	1	D	.00279	-27.6
			.00211	-24.8
			.00384	-27.1
			.00302	-24.7
14	1	E	.00264	-23.3
			.00138	-36.9
			.00092	-28.6
			.00043	-20.7
15	1	F	.00147	-29.2
			.00096	-23.5
			.00059	-19.6
			.00201	-28.6
16	2	G	.00148	-24.1
			.00115	-21.2
			.00263	-28.7
			.00189	-23.4
17	2	H	.00144	-20.4
			.00223	-30.7
			.00164	-25.9
			.00118	-21.7
18	2	I	.00261	-31.0
			.00212	-26.4
			.00181	-23.9
			.00141	-19.7
19	2	J	.00251	-30.2
			.00209	-26.3
			.00148	-21.2
			.00090	-17.7
20	5	K		
21	5	L		

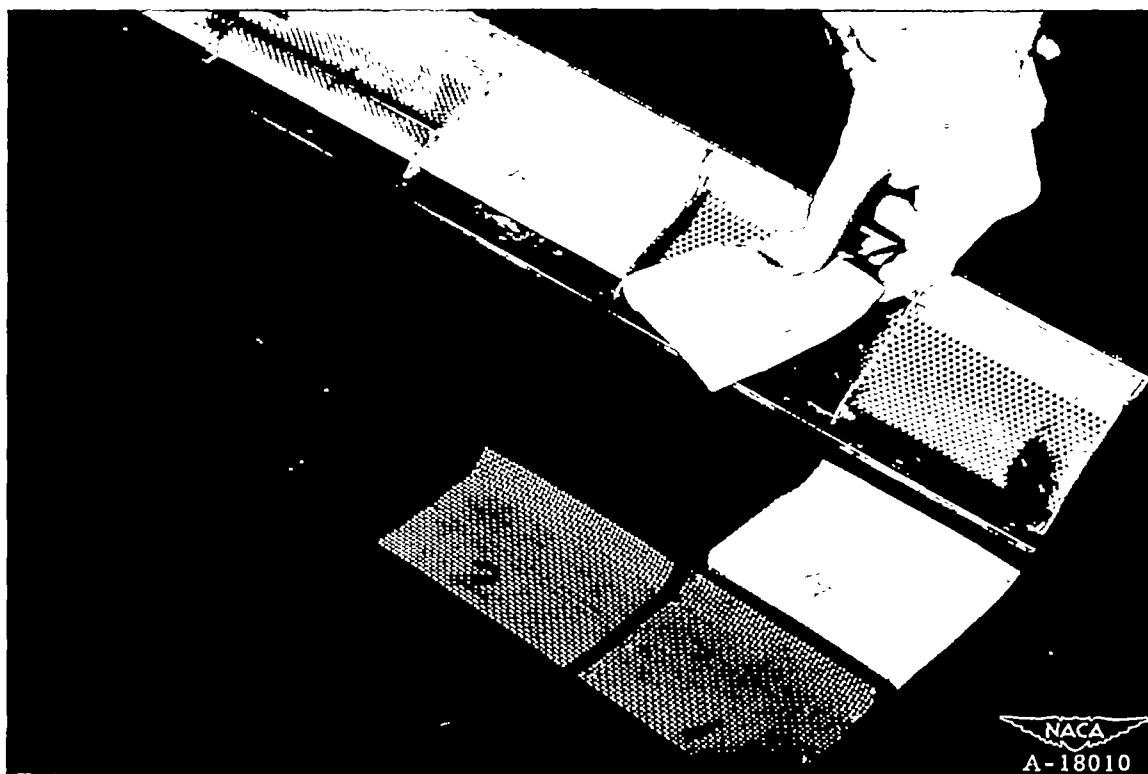




Figure 1.— The 10.51-percent-thick symmetrical airfoil with a porous leading edge.

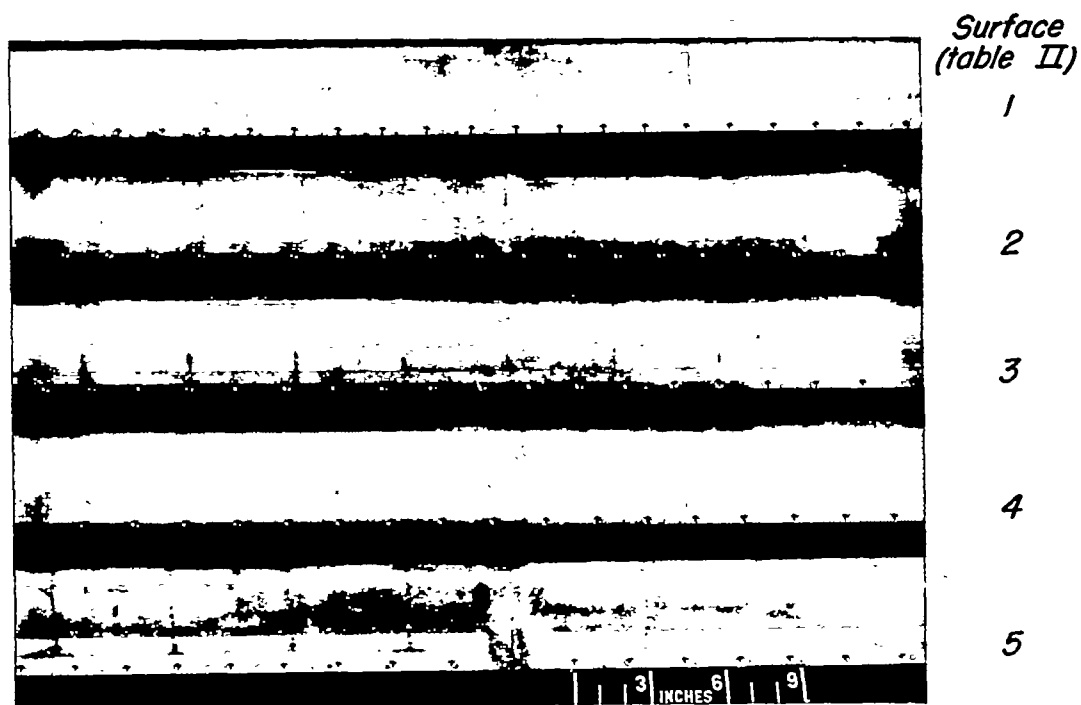


(a) Section through the model.



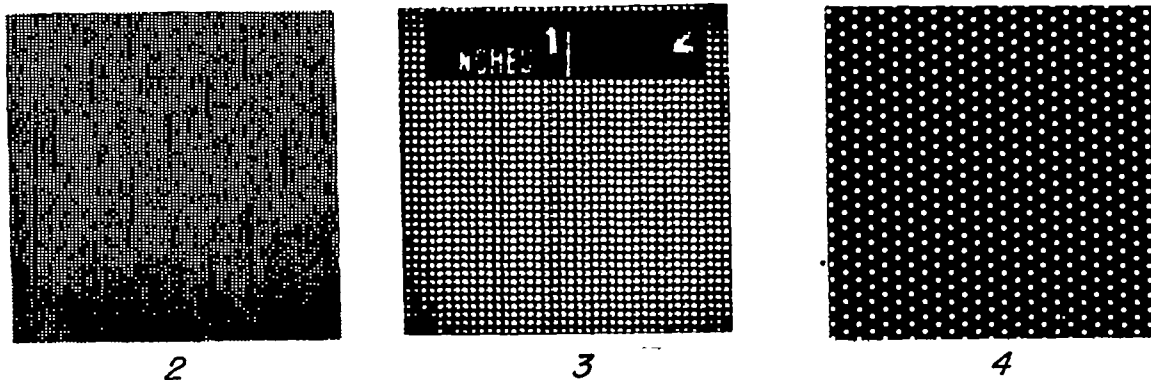
(b) Typical arrangement of the permeable material (felt) in a perforated-plate nose section.

Figure 2.—Detail of model construction.



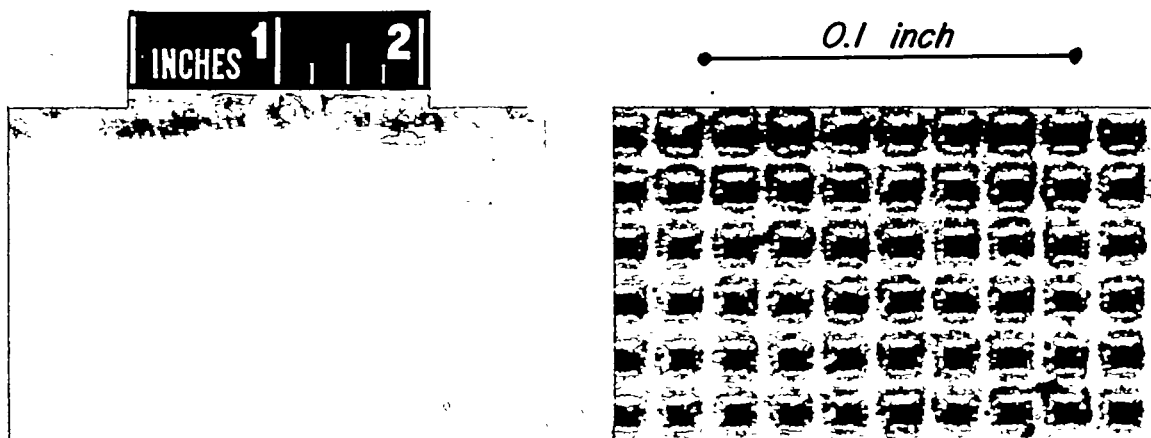
A-18009

(a) The leading-edge sections tested.

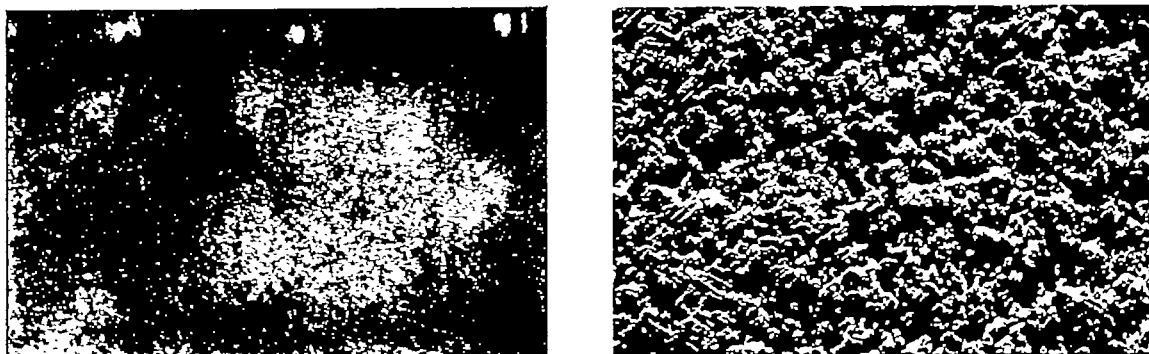


(b) Perforated plates 2, 3, and 4.

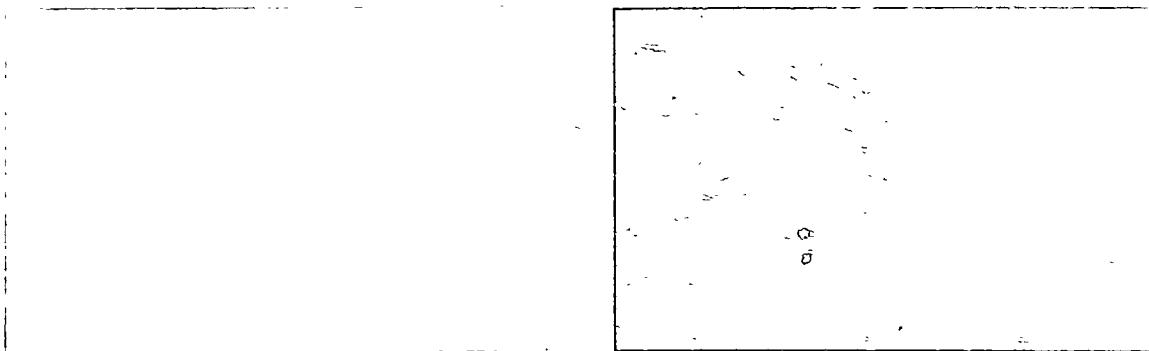
Figure 3.—Details of surface material.



Perforated plate 1



Sintered steel (material 5, table II)



Filter paper, ref. 1 (material 7, table II)



(c) Surface materials 1, 5, and 7. Magnification ratio is 21X.

Figure 3.- Concluded.

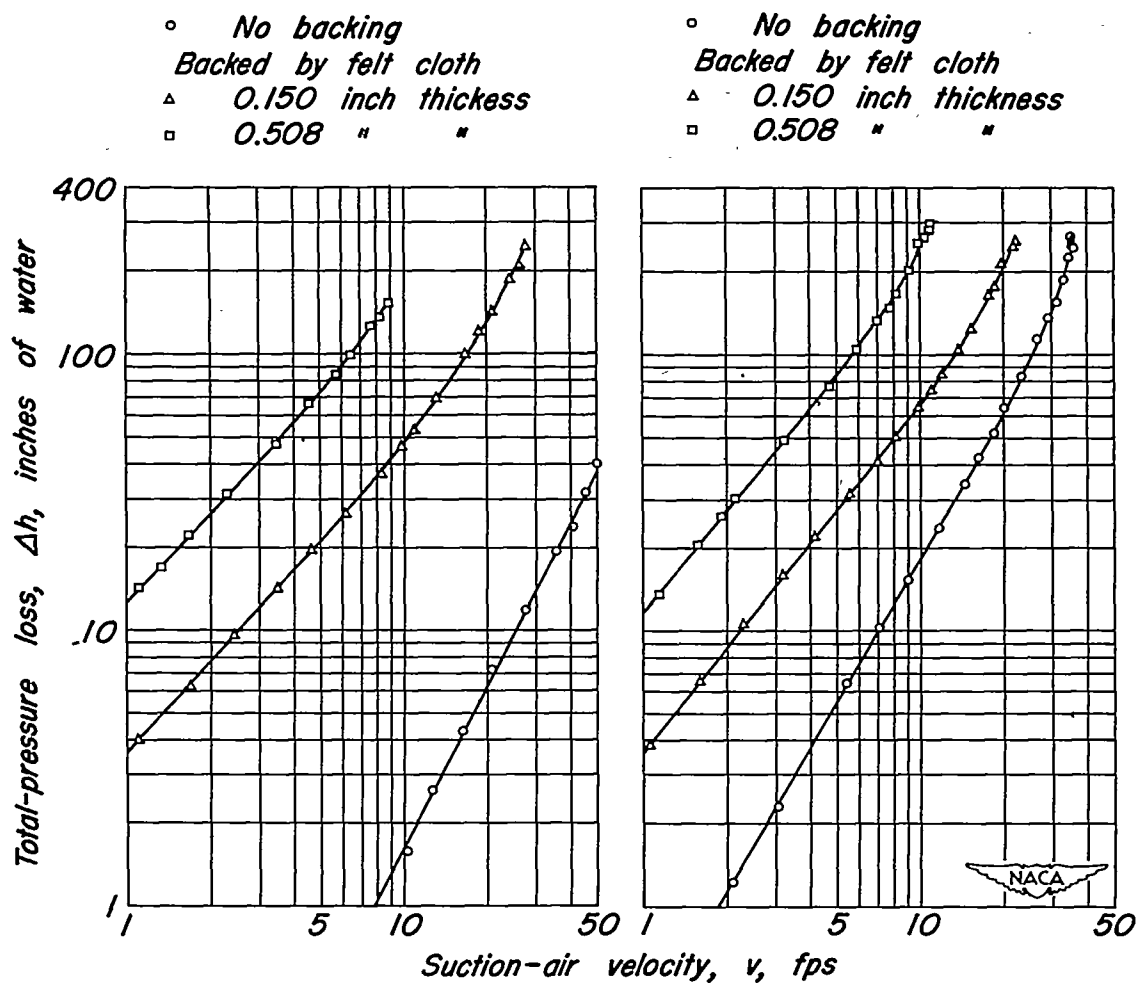


Figure 4.- Flow resistance at the start of the tests of the porous materials used.

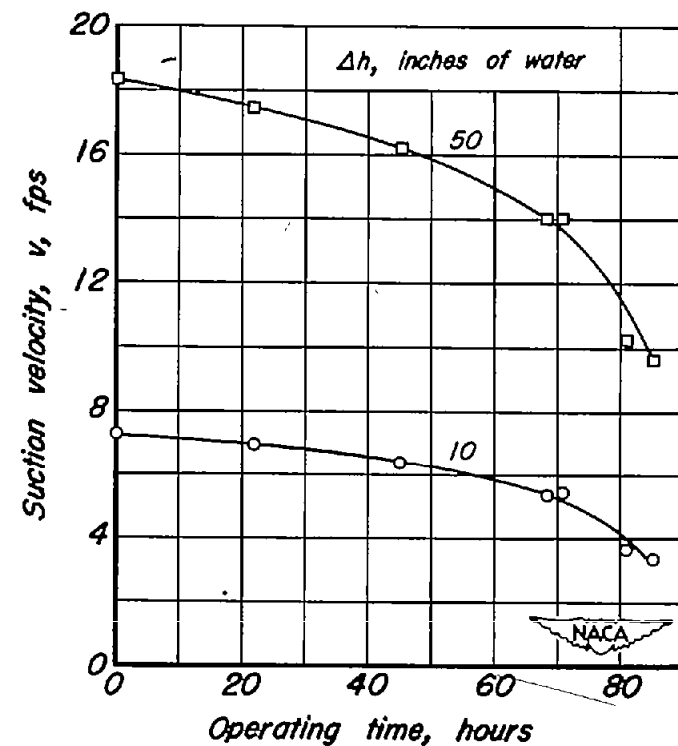
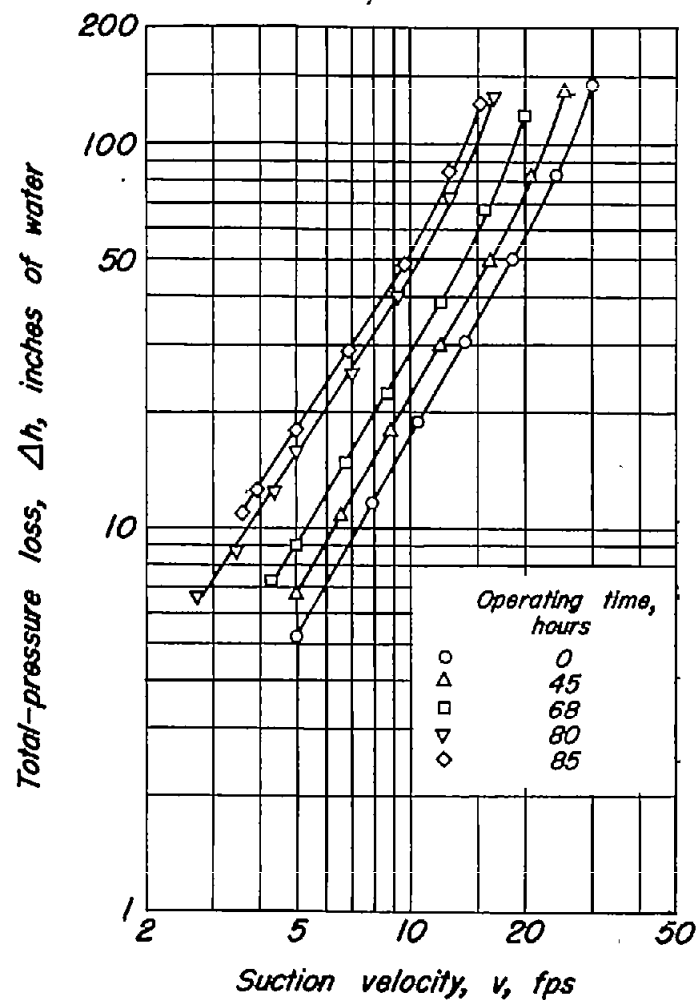


Figure 5.-Effect of clogging on the flow-resistance characteristics of sintered steel (surface material 5).

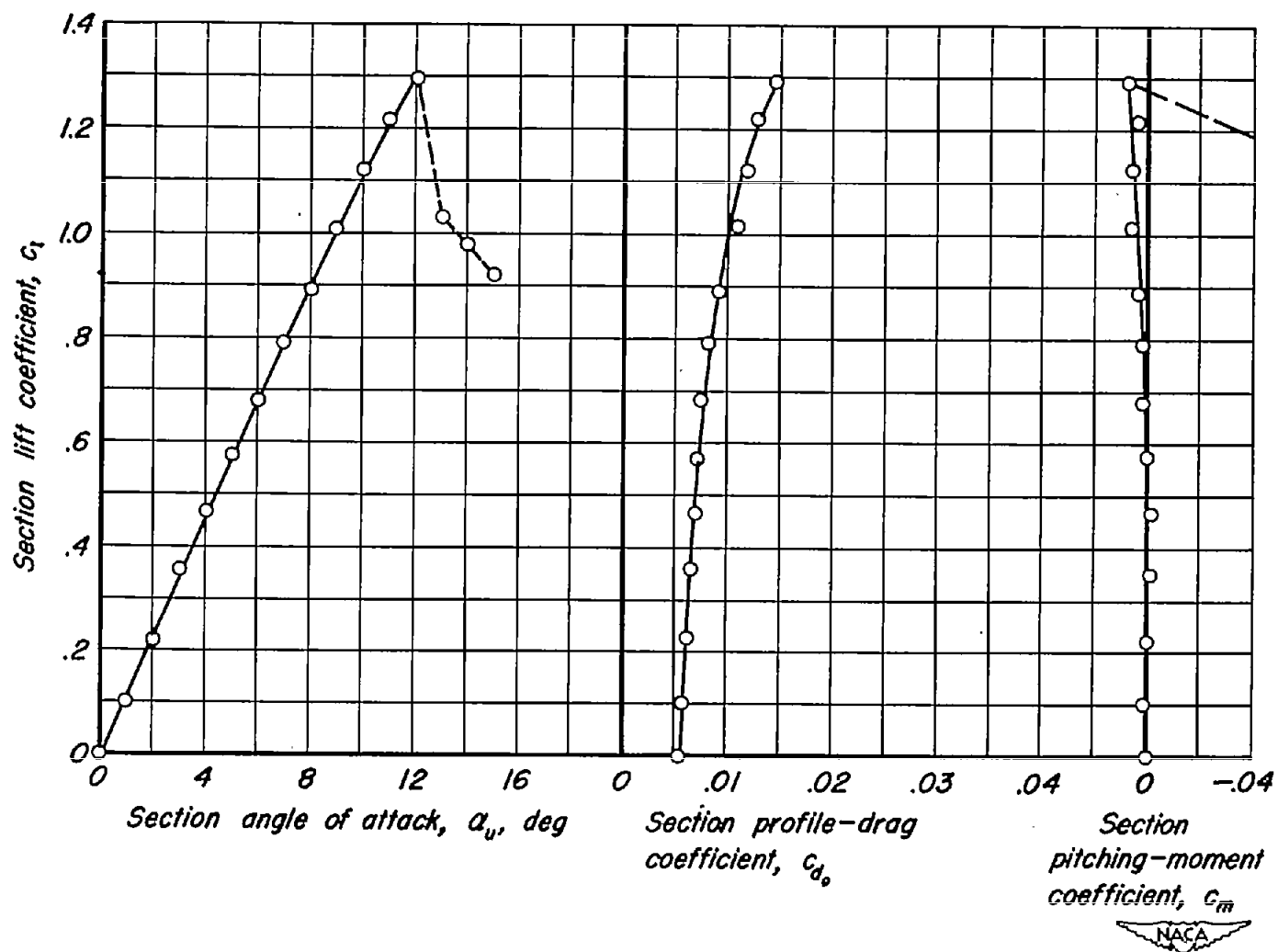


Figure 6.- Section aerodynamic characteristics of the plain airfoil. $U_0=162$ fps.

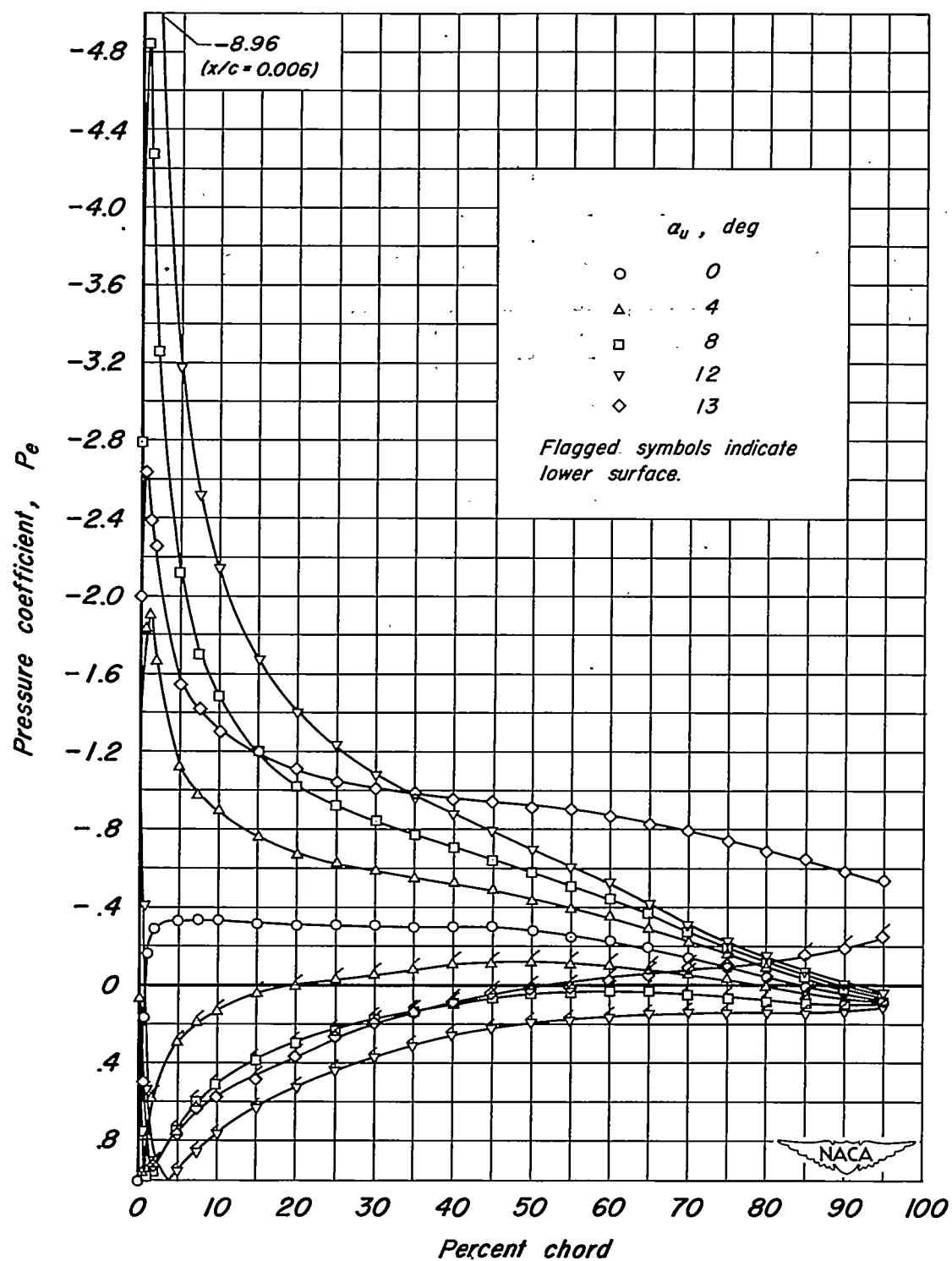


Figure 7.- Chordwise distribution of pressure over the plain airfoil.
 $U_0 = 162$ fps.

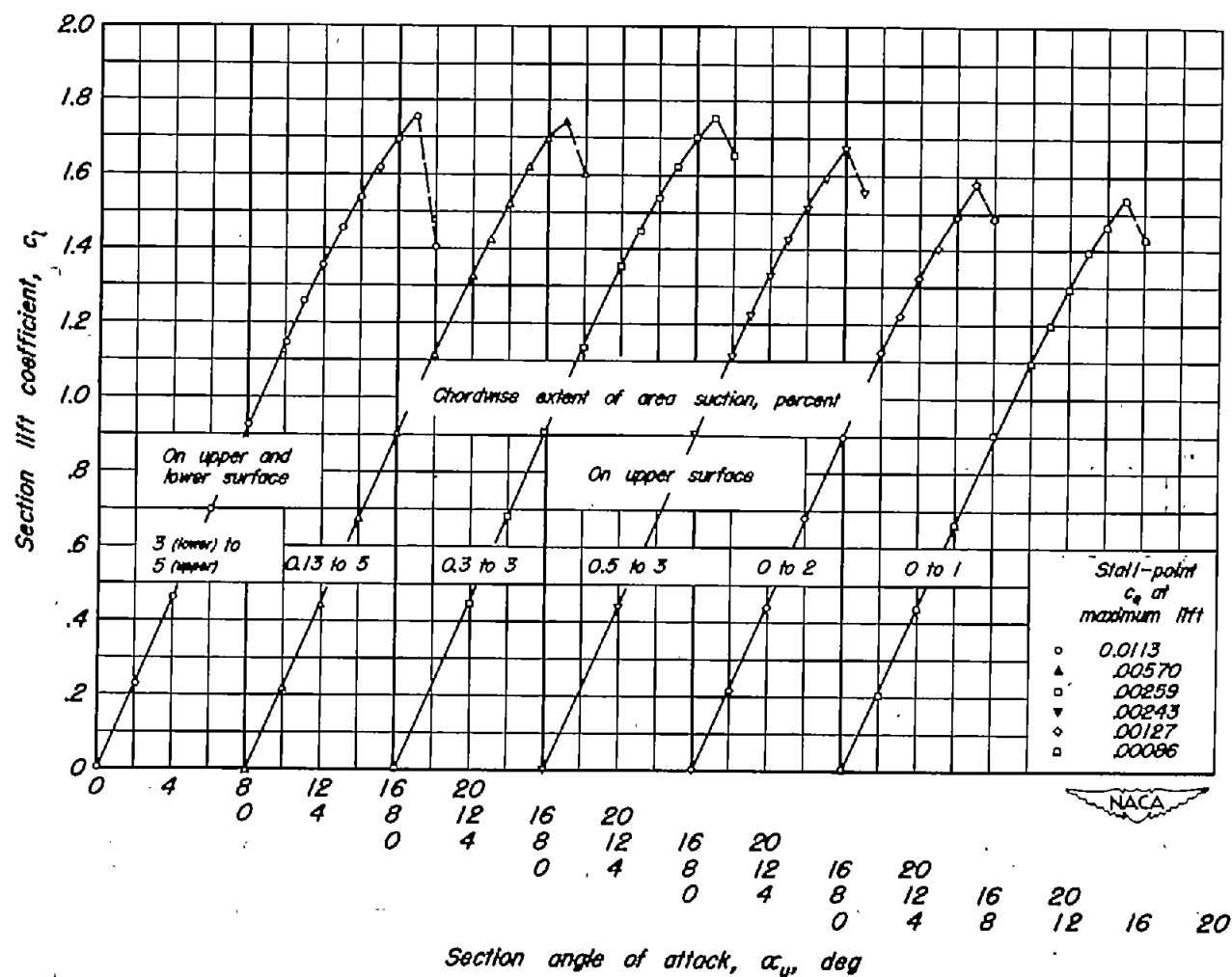


Figure 8.-Lift characteristics of the model for various chordwise extents of area suction.
 $U_o = 162$ fps.

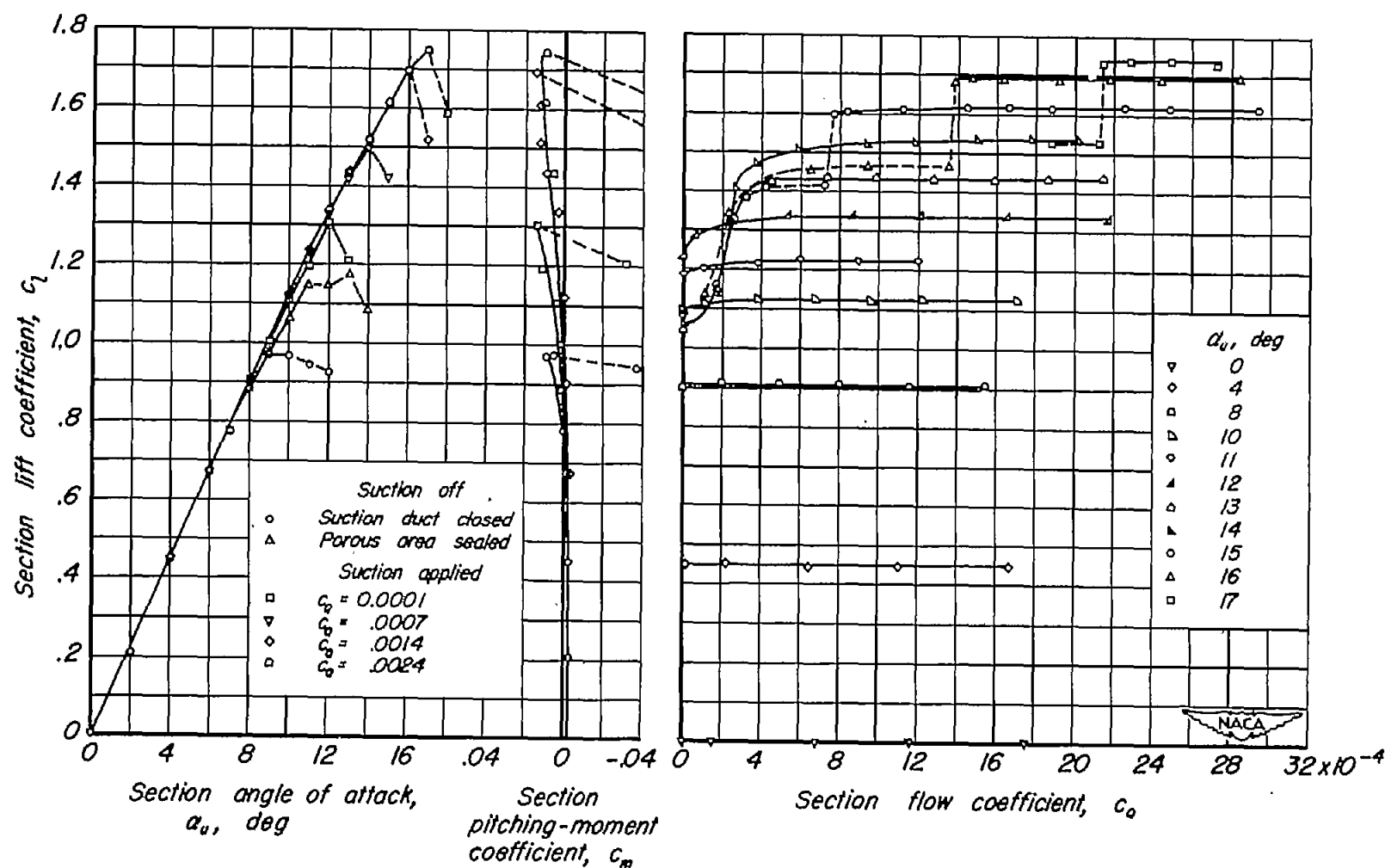
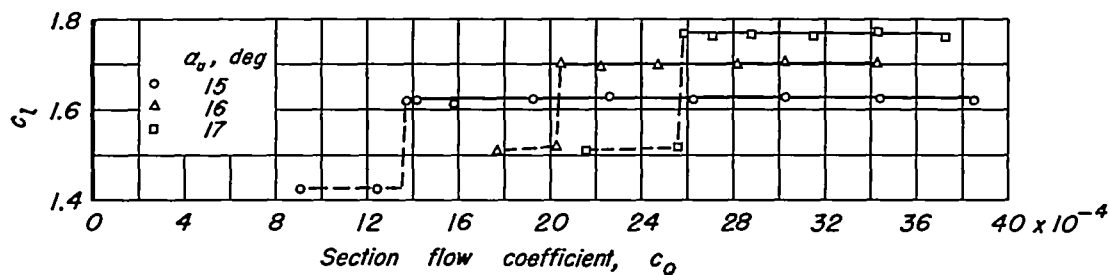
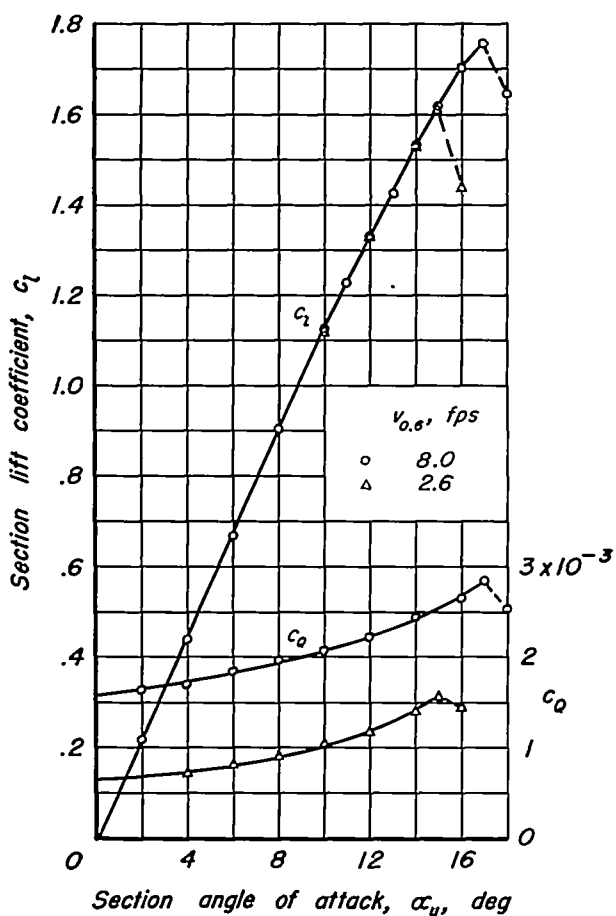


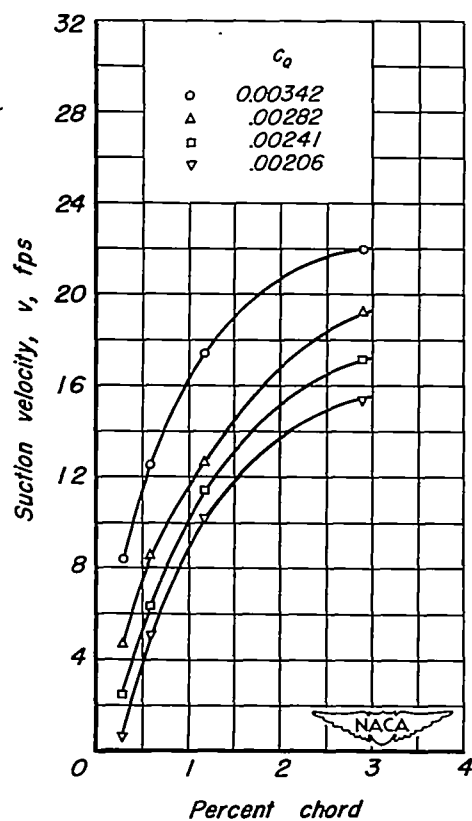
Figure 9.- Effect of suction on the lift and moment characteristics of the model with perforated plate 1 and permeability arrangement G. $U_o = 162$ fps.



(a) Constant angle of attack.

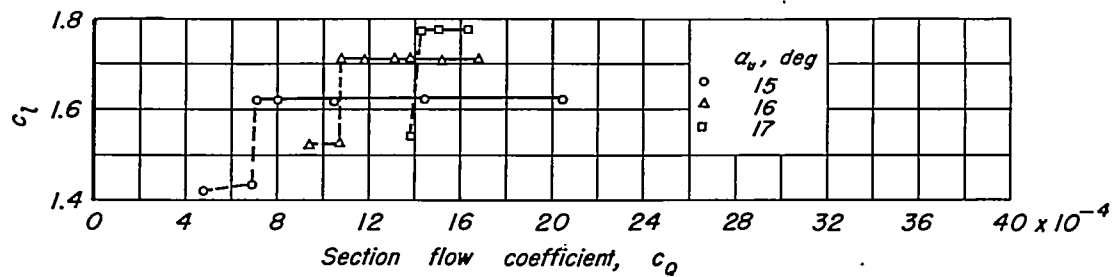


(b) Constant suction velocity.

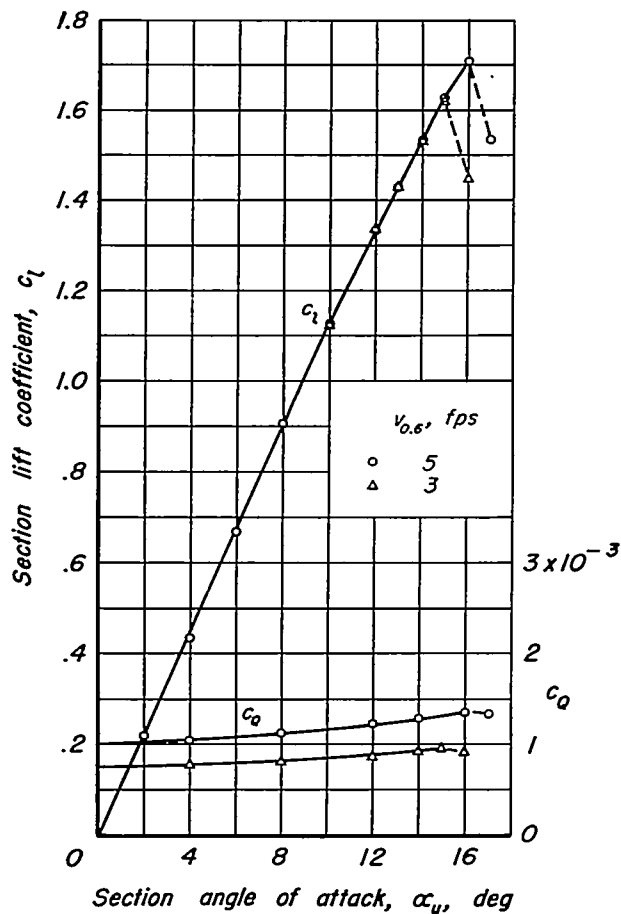


(c) Suction-velocity distribution, $\alpha_u = 16^\circ$.

Figure 10.- Lift and flow characteristics of the model with perforated plate 1 and permeability arrangement A. $U_0 = 162$ fps.



(a) Constant angle of attack.



(b) Constant suction velocity.

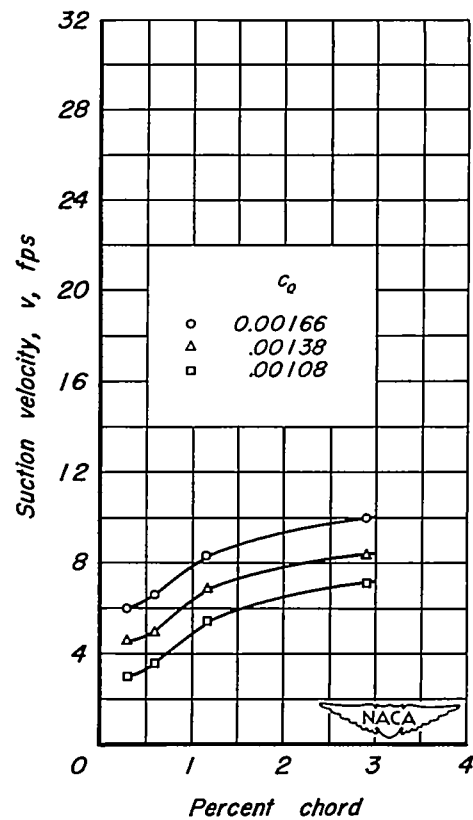
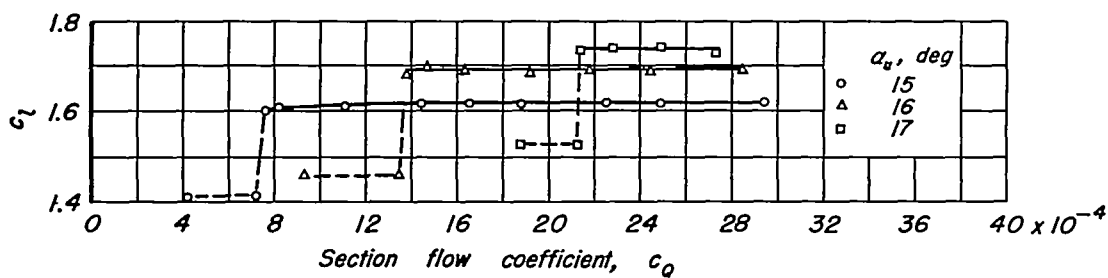
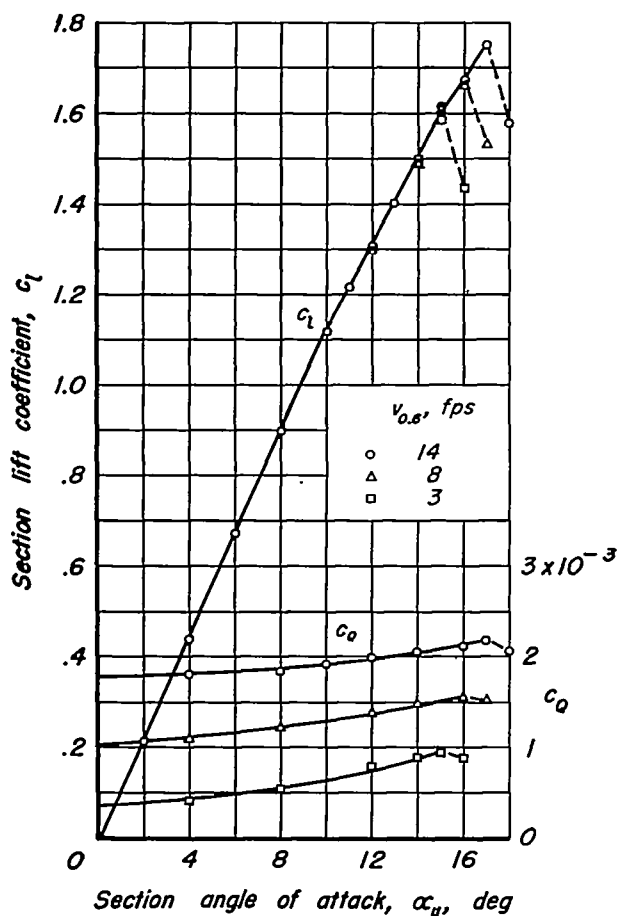
(c) Suction-velocity distribution, $\alpha_u = 16^\circ$.

Figure 11.- Lift and flow characteristics of the model with perforated plate I and permeability arrangement B. $U_0 = 162$ fps.



(a) Constant angle of attack.



(b) Constant suction velocity.

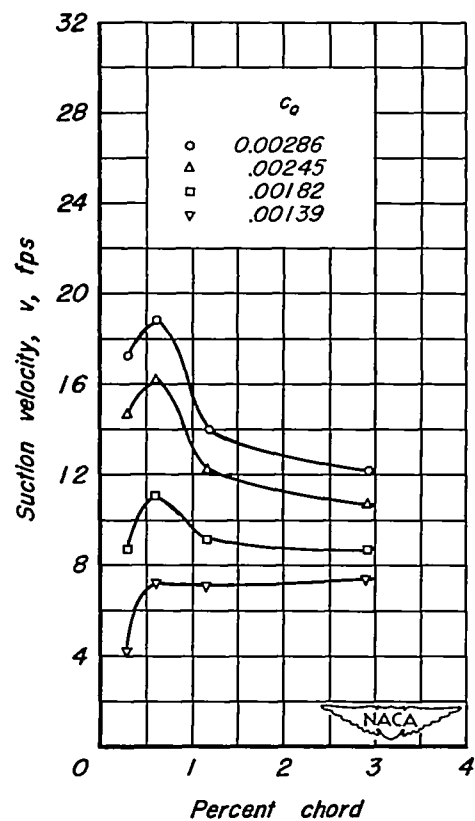
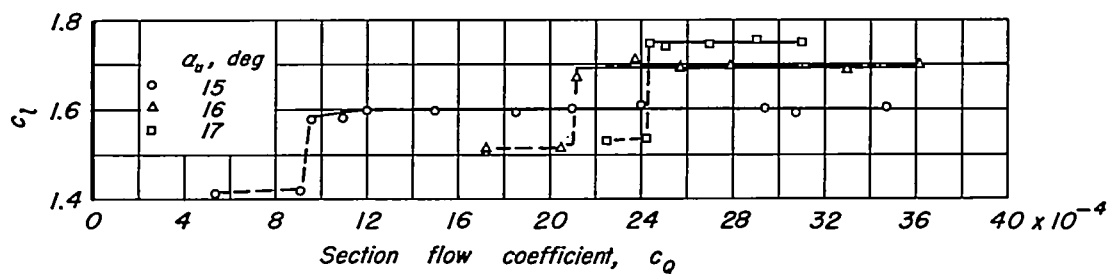
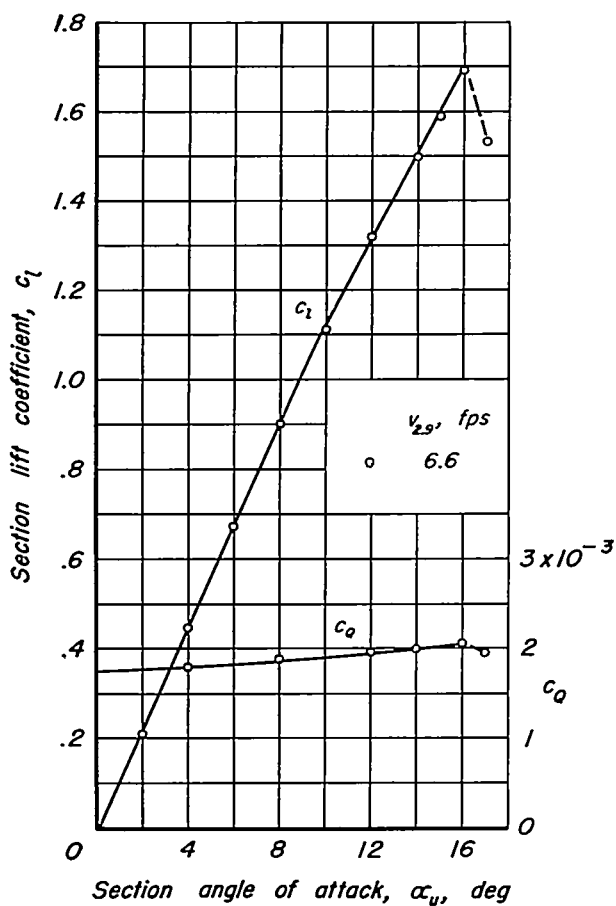
(c) Suction-velocity distribution, $\alpha_a = 16^\circ$.

Figure 12.- Lift and flow characteristics of the model with perforated plate 1 and permeability arrangement C. $U_0 = 162$ fps.



(a) Constant angle of attack.



(b) Constant suction velocity.

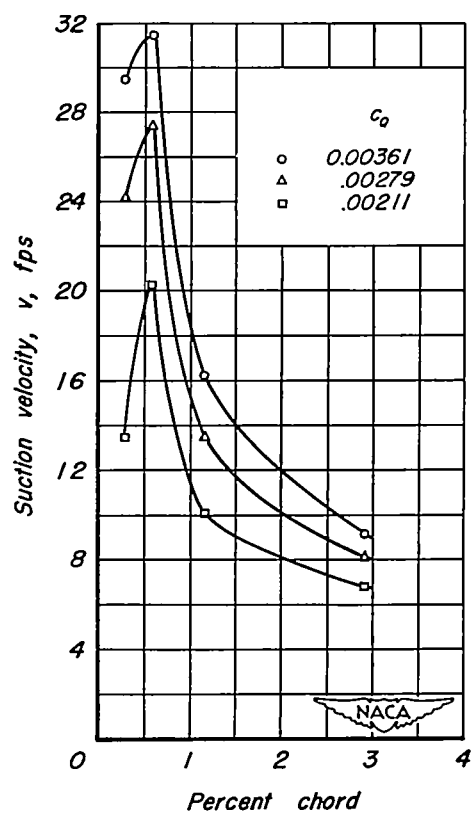
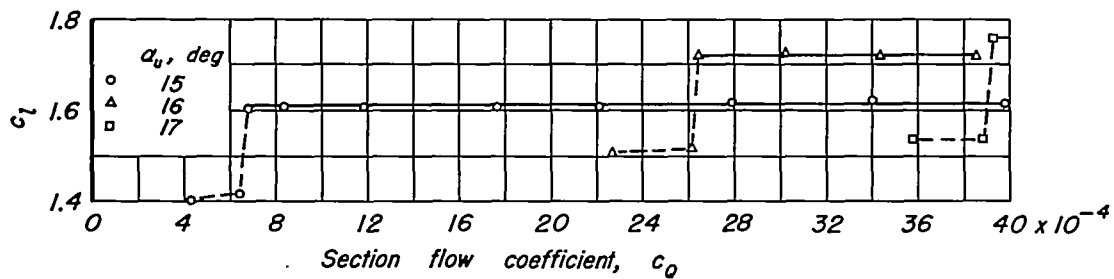
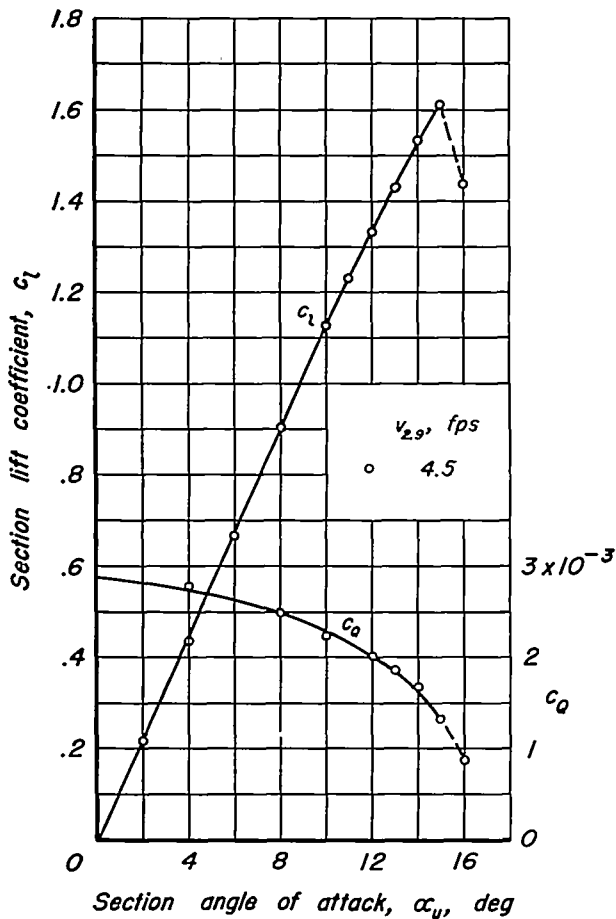
(c) Suction-velocity distribution, $\alpha_a = 16^\circ$.

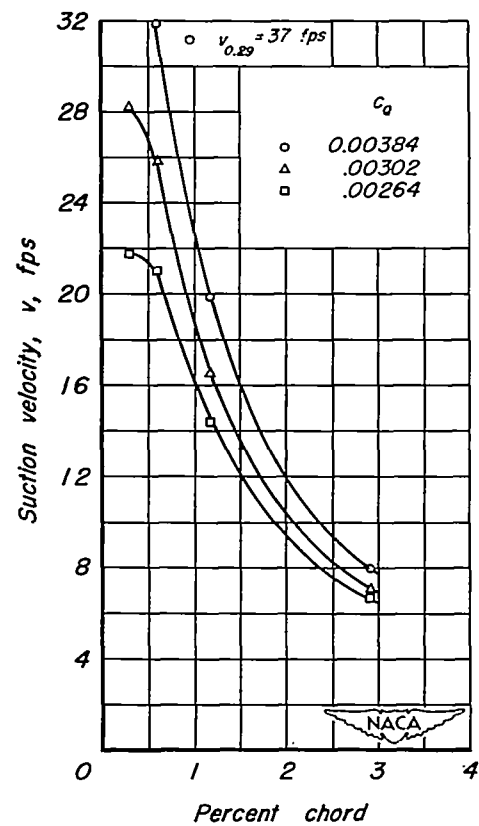
Figure 13.- Lift and flow characteristics of the model with perforated plate I and permeability arrangement D. $U_o = 162$ fps.

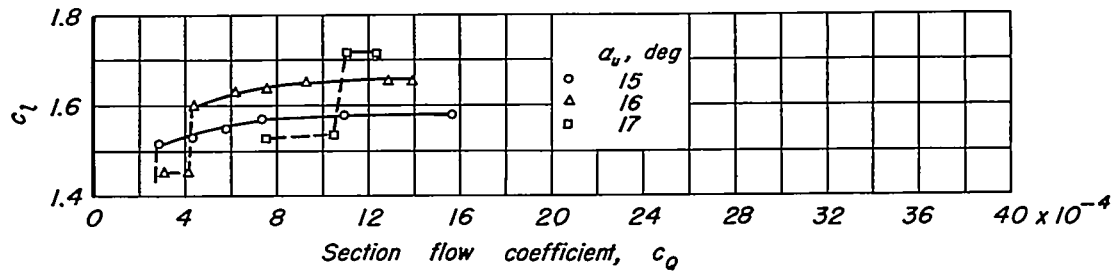


(a) Constant angle of attack.

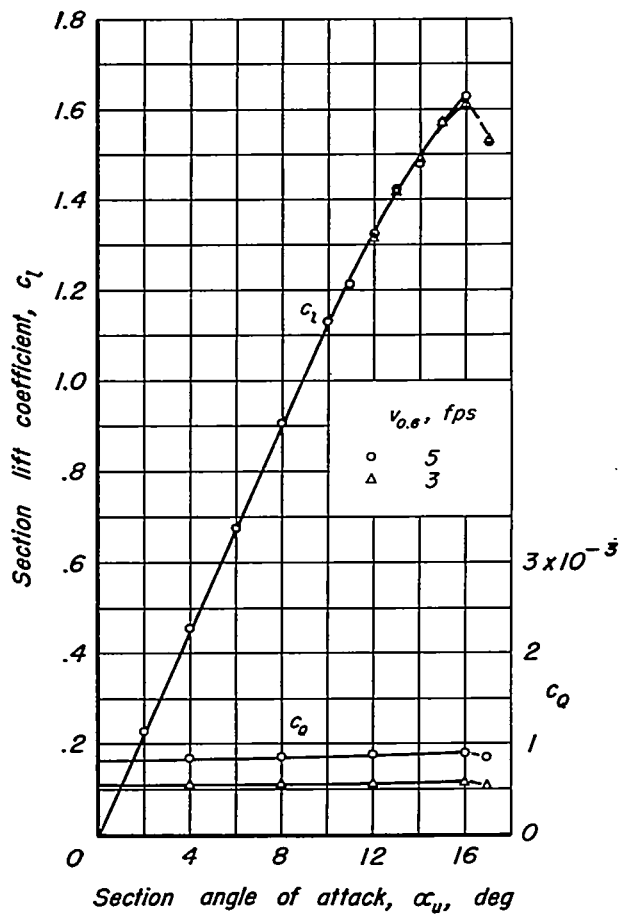


(b) Constant suction velocity.

(c) Suction-velocity distribution, $\alpha_u = 16^\circ$.Figure 14.- Lift and flow characteristics of the model with perforated plate 1 and permeability arrangement E. $U_o = 162$ fps.



(a) Constant angle of attack.



(b) Constant suction velocity.

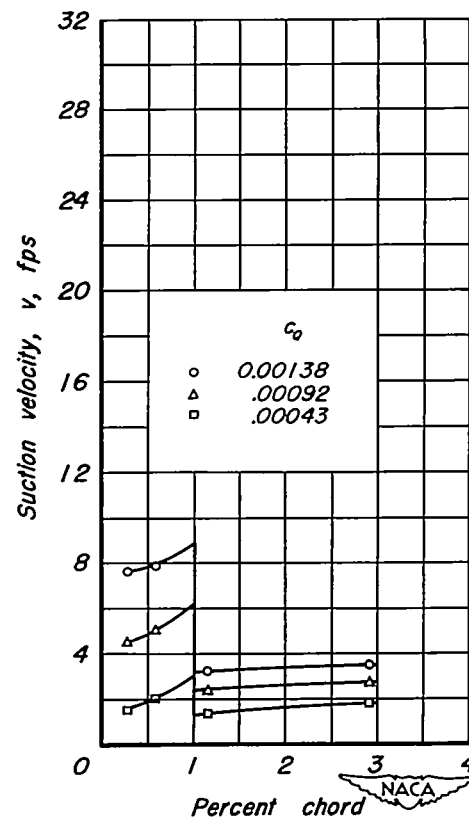
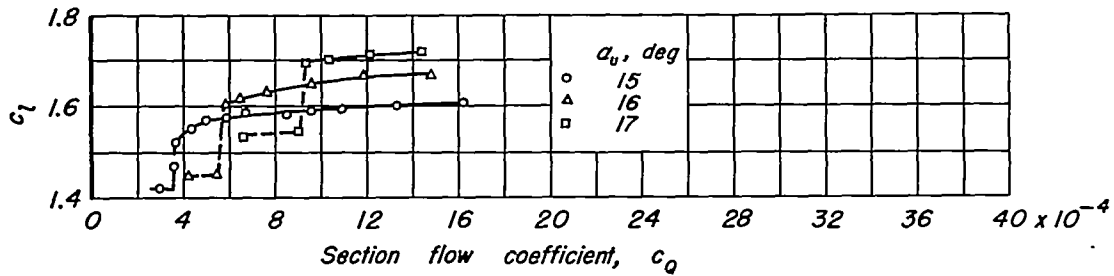
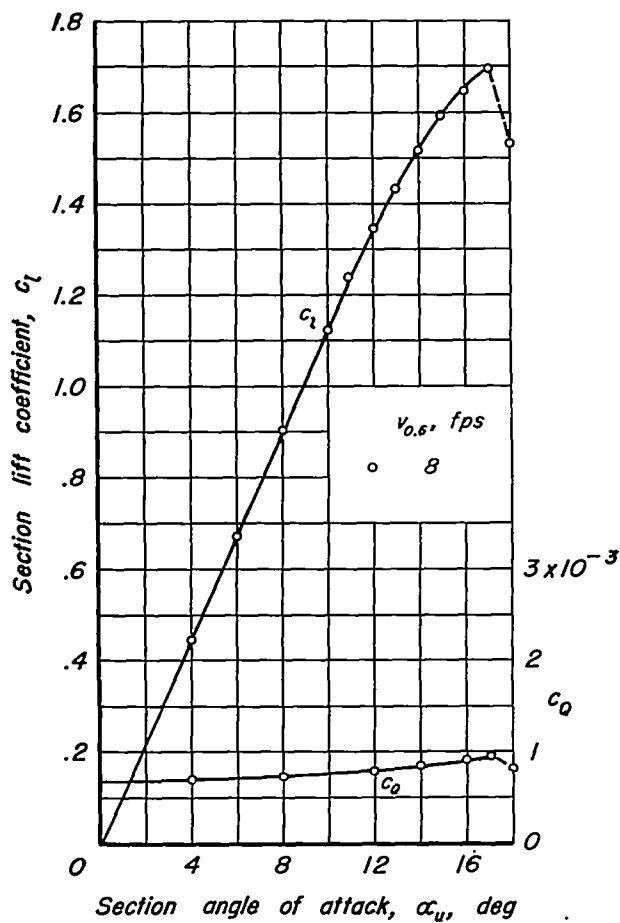
(c) Suction-velocity distribution, $\alpha_u = 16^\circ$.

Figure 15.- Lift and flow characteristics of the model with perforated plate I and permeability arrangement F. $U_0 = 162$ fps.



(a) Constant angle of attack.



(b) Constant suction velocity.

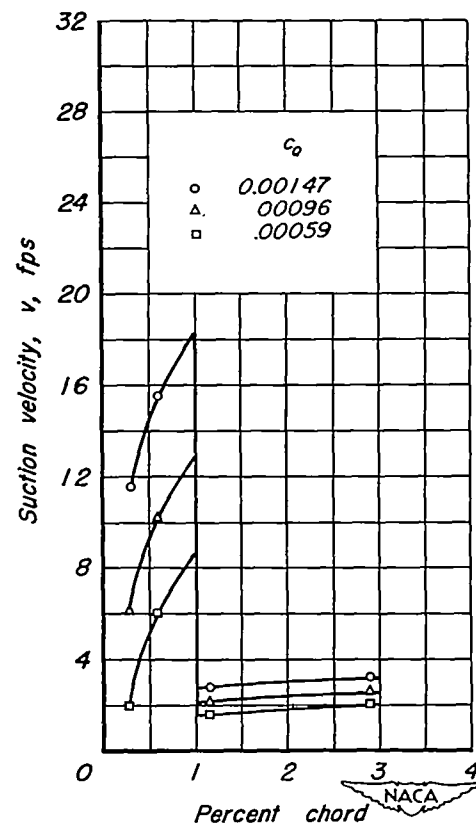
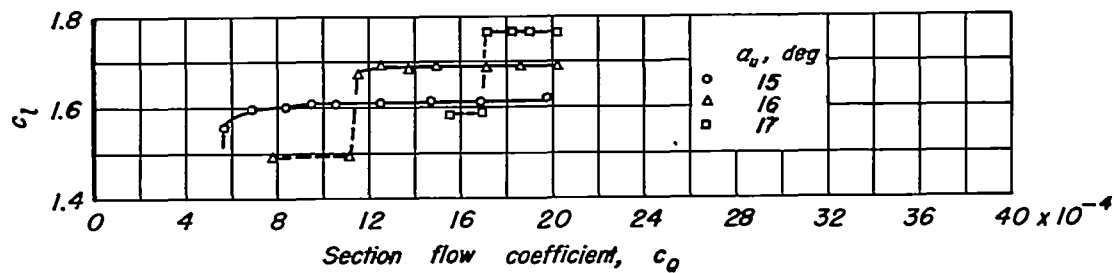
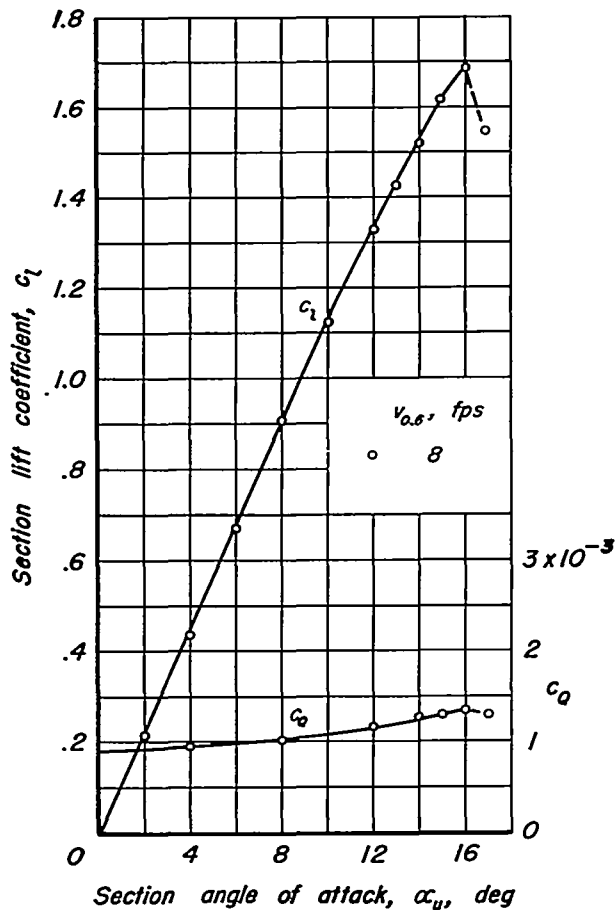
(c) Suction-velocity distribution, $\alpha_u = 16^\circ$.

Figure 16.- Lift and flow characteristics of the model with perforated plate 2 and permeability arrangement G. $U_0 = 162$ fps.



(a) Constant angle of attack.



(b) Constant suction velocity.

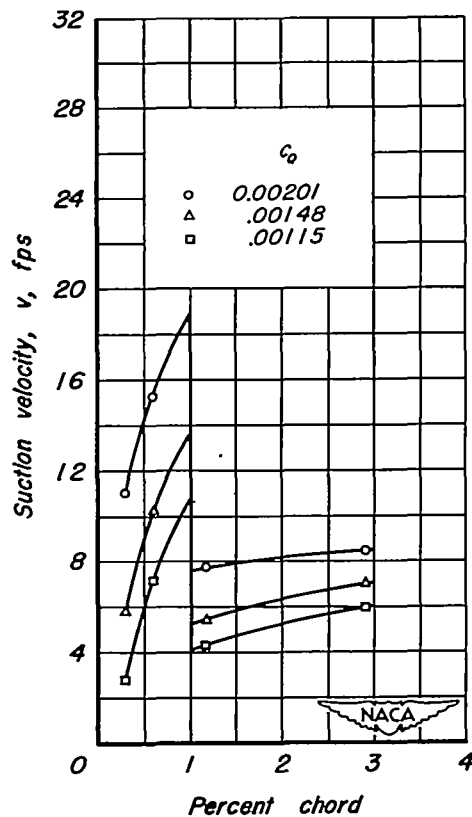
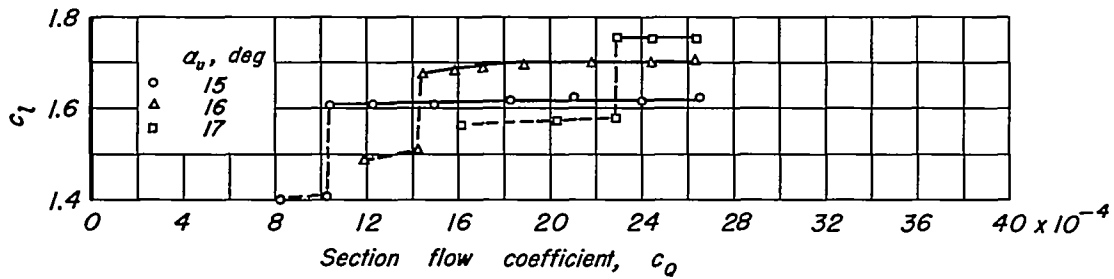
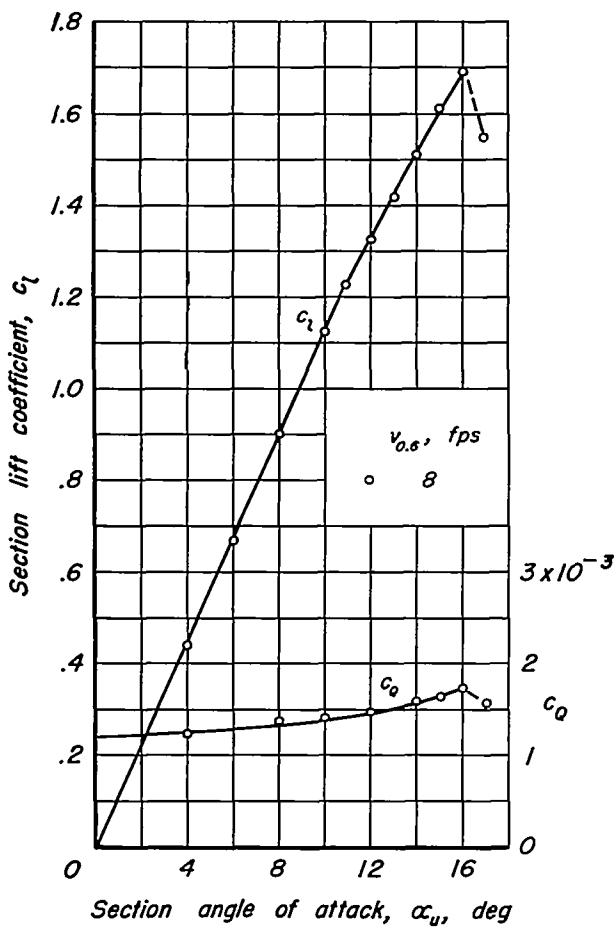
(c) Suction-velocity distribution, $\alpha_u = 16^\circ$.

Figure 17.- Lift and flow characteristics of the model with perforated plate 2 and permeability arrangement H. $U_0 = 162$ fps.



(a) Constant angle of attack.



(b) Constant suction velocity.

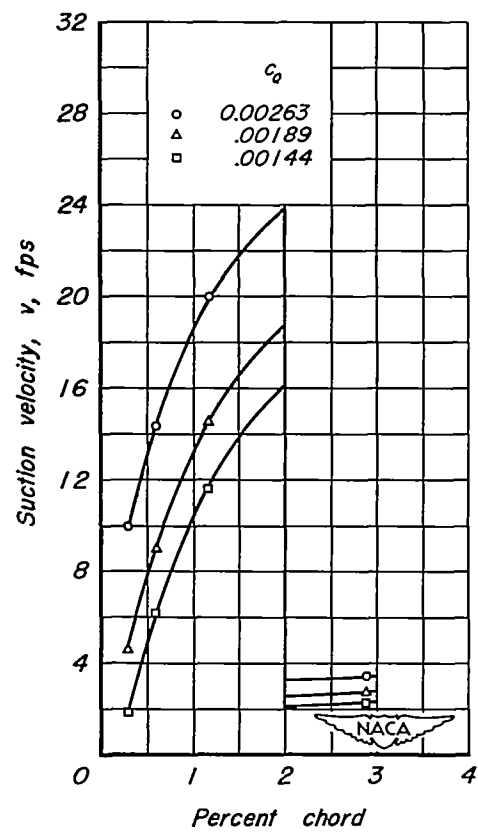
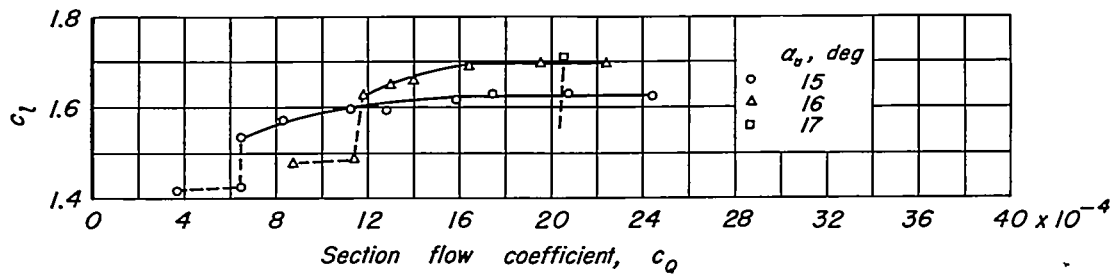
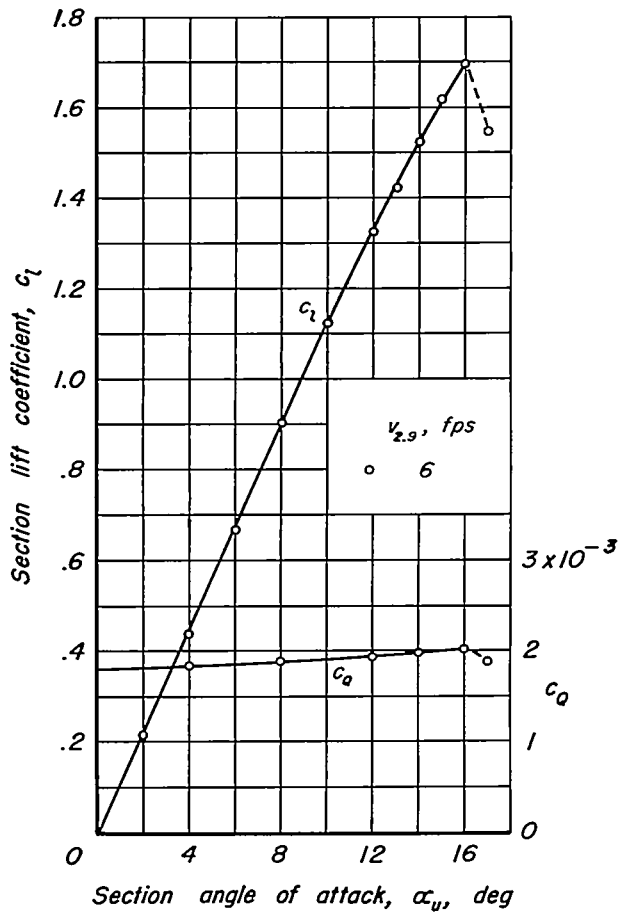
(c) Suction-velocity distribution, $\alpha_u = 16^\circ$.

Figure 1B - Lift and flow characteristics of the model with perforated plate 2 and permeability arrangement I. $U_0 = 162$ fps.



(a) Constant angle of attack.



(b) Constant suction velocity.

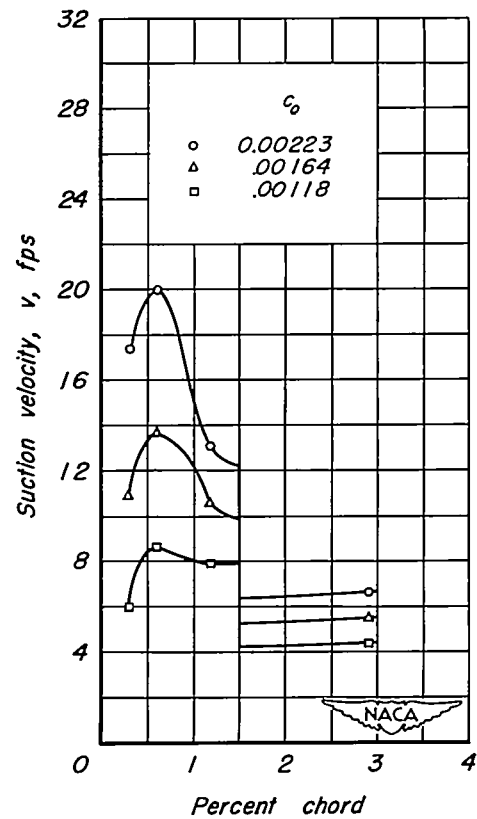
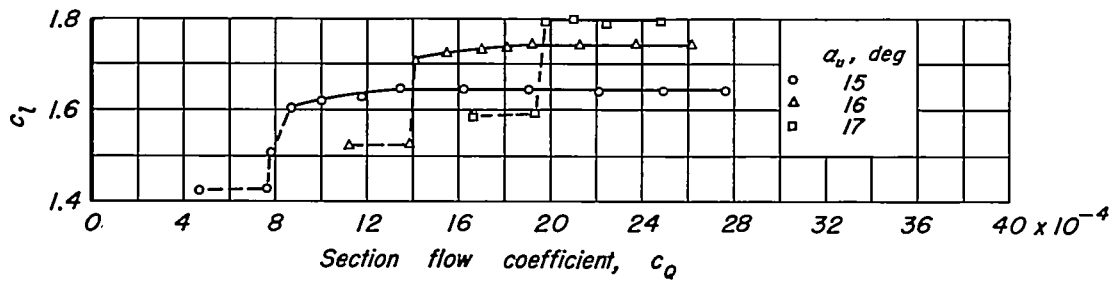
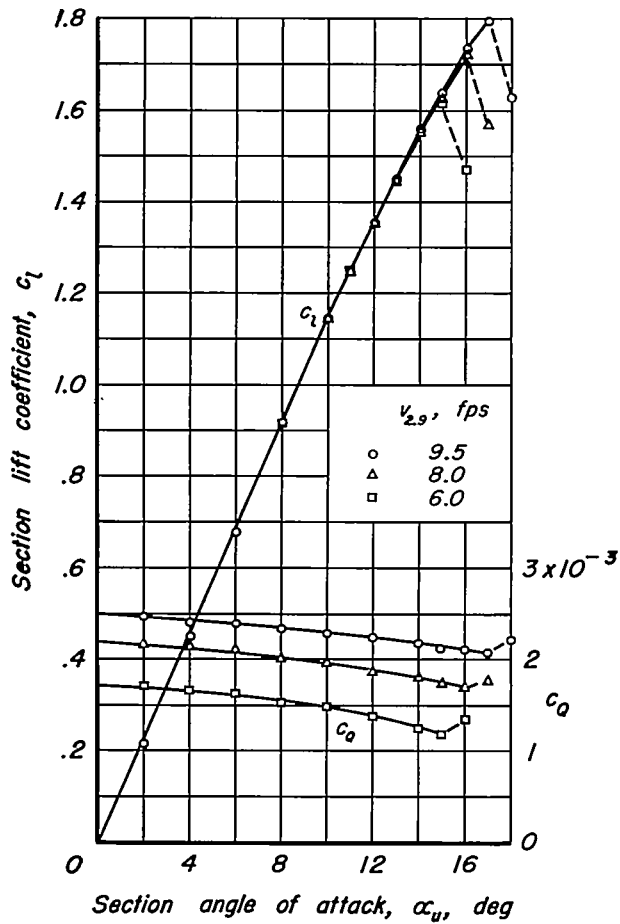
(c) Suction-velocity distribution, $\alpha_u = 16^\circ$.

Figure 19.- Lift and flow characteristics of the model with perforated plate 2 and permeability arrangement J. $U_o = 162$ fps.



(a) Constant angle of attack.



(b) Constant suction velocity.

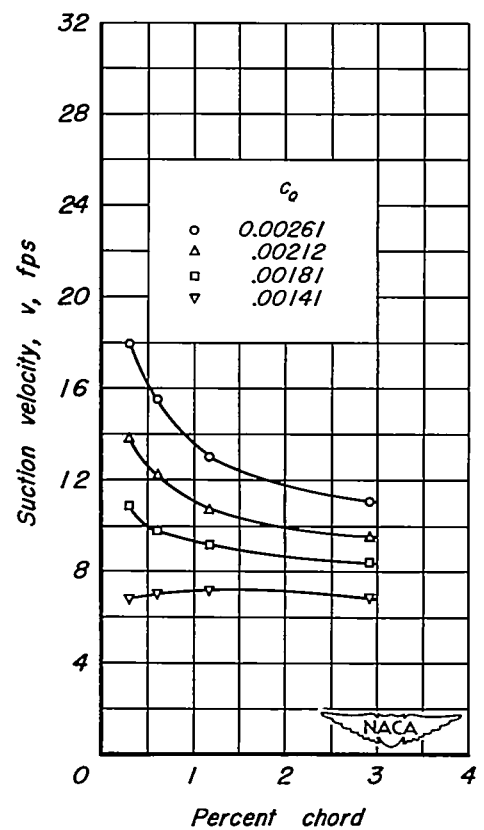
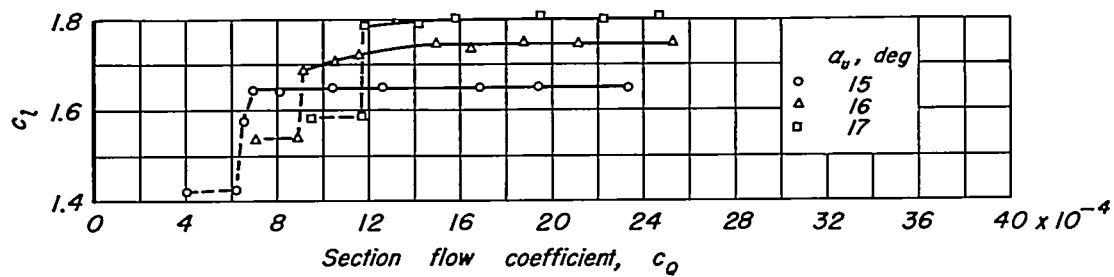
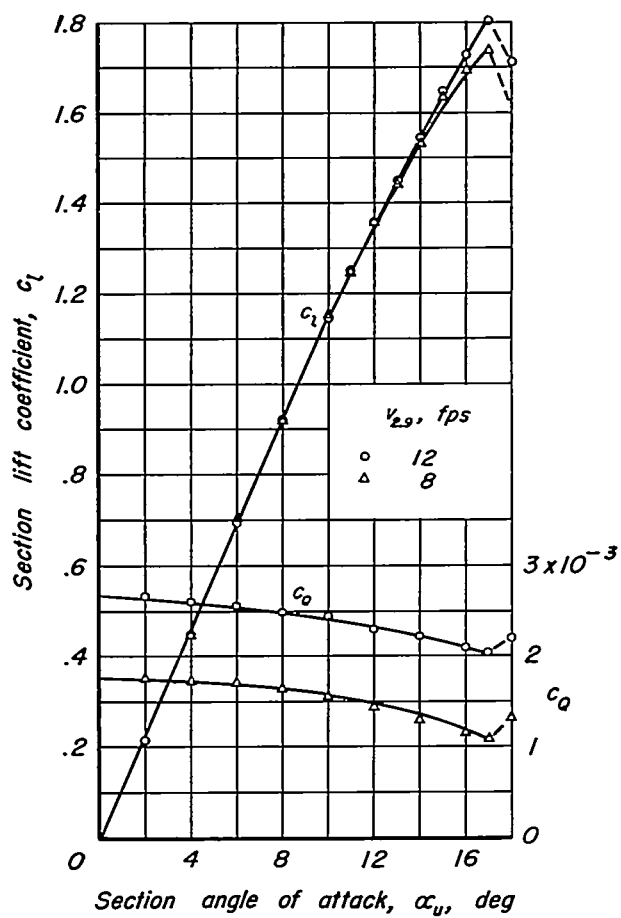
(c) Suction-velocity distribution, $\alpha_u = 16^\circ$.

Figure 20.- Lift and flow characteristics of the model with sintered steel and permeability arrangement K. $U_0 = 162$ fps.



(a) Constant angle of attack.



(b) Constant suction velocity.

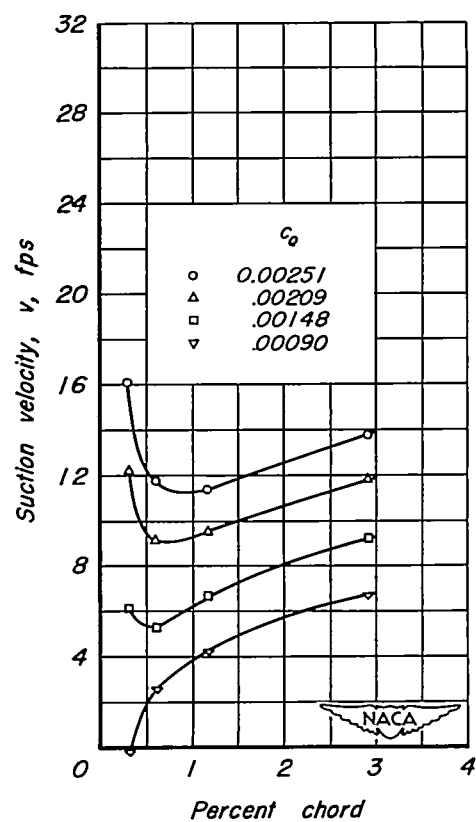
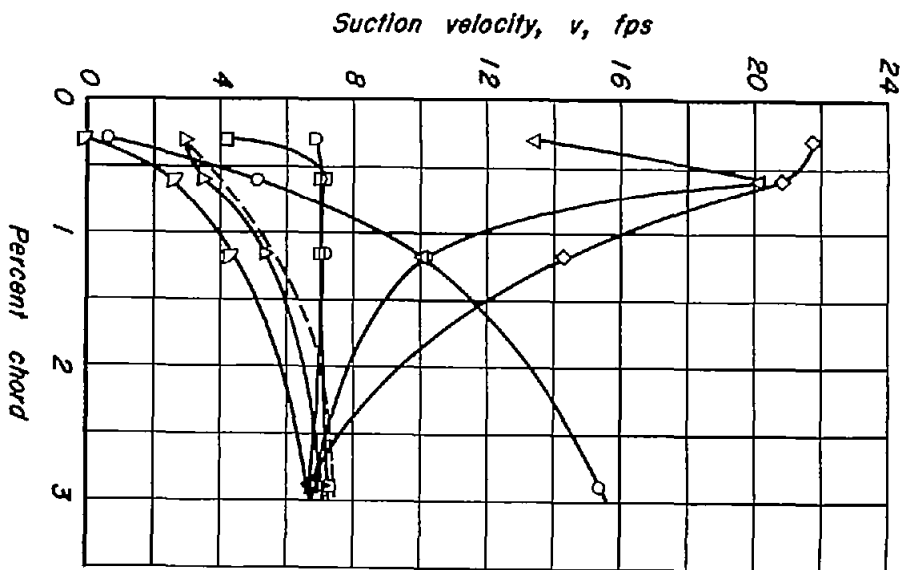
(c) Suction-velocity distribution, $\alpha_u = 16^\circ$.

Figure 21.-Lift and flow characteristics of the model with sintered steel and permeability arrangement L. $U_o = 162$ fps.



Surface	Permeability	c_q	c_t	P
Perforated plate	A	0.00206	1.70	-19.7
"	B	.00108	1.71	-24.7
"	C	.00139	1.69	-20.8
"	D	.00211	1.69	-24.8
"	E	.00264	1.72	-23.3
Sintered steel	K	.00141	1.71	-19.7
"	L	.00090	1.69	-17.7
Filler paper (ref. 1)	M	.00119	1.71	-19.9



Figure 22 - Stall-point suction velocity distributions for smooth-type permeability arrangements. $\alpha_a = 16^\circ$, $U_0 = 162$ fps.

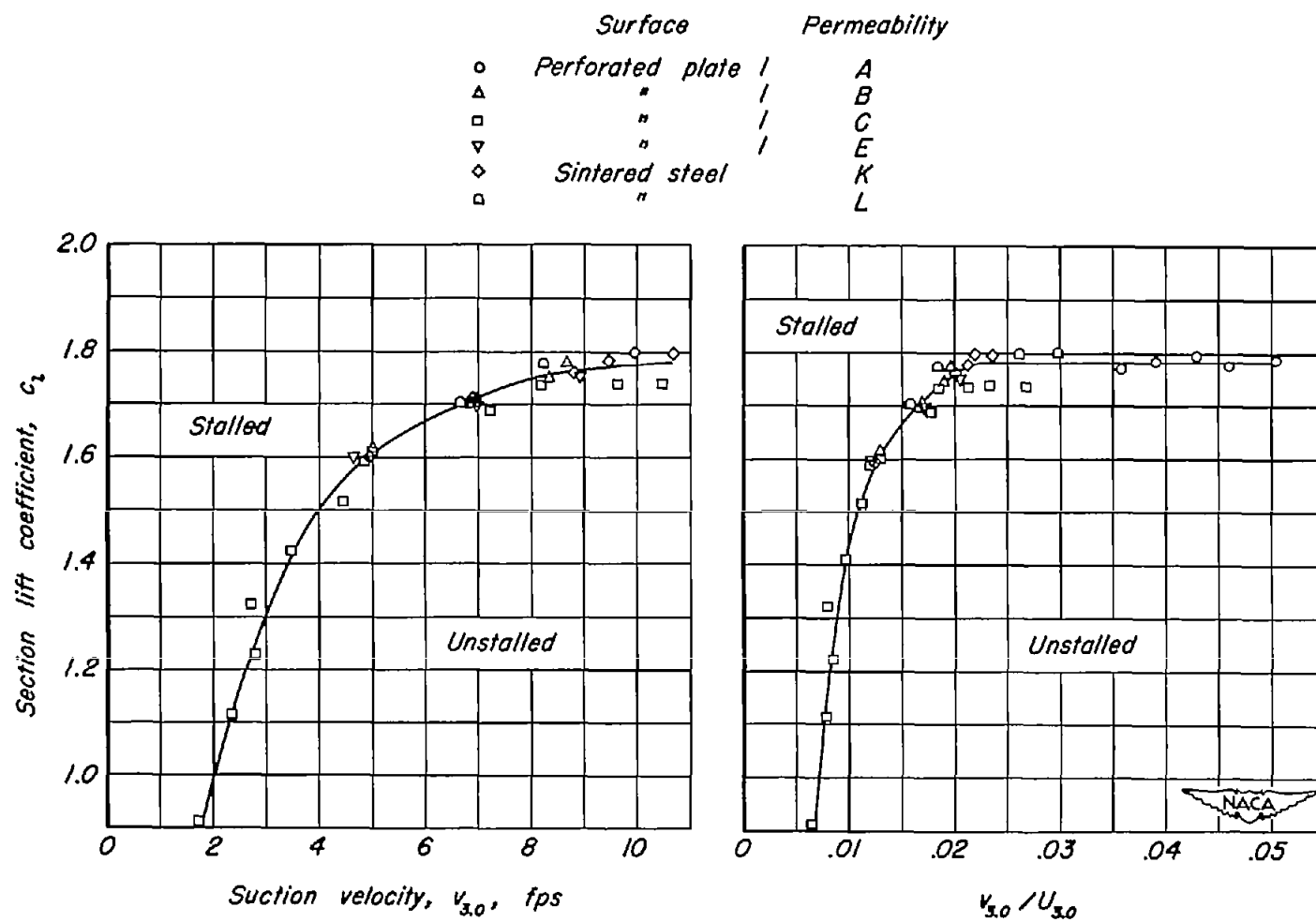


Figure 23.- Variation of stall-point suction velocity at 3-percent chord with section lift coefficient for smooth-type permeability arrangements. $U_0 = 162$ fps.

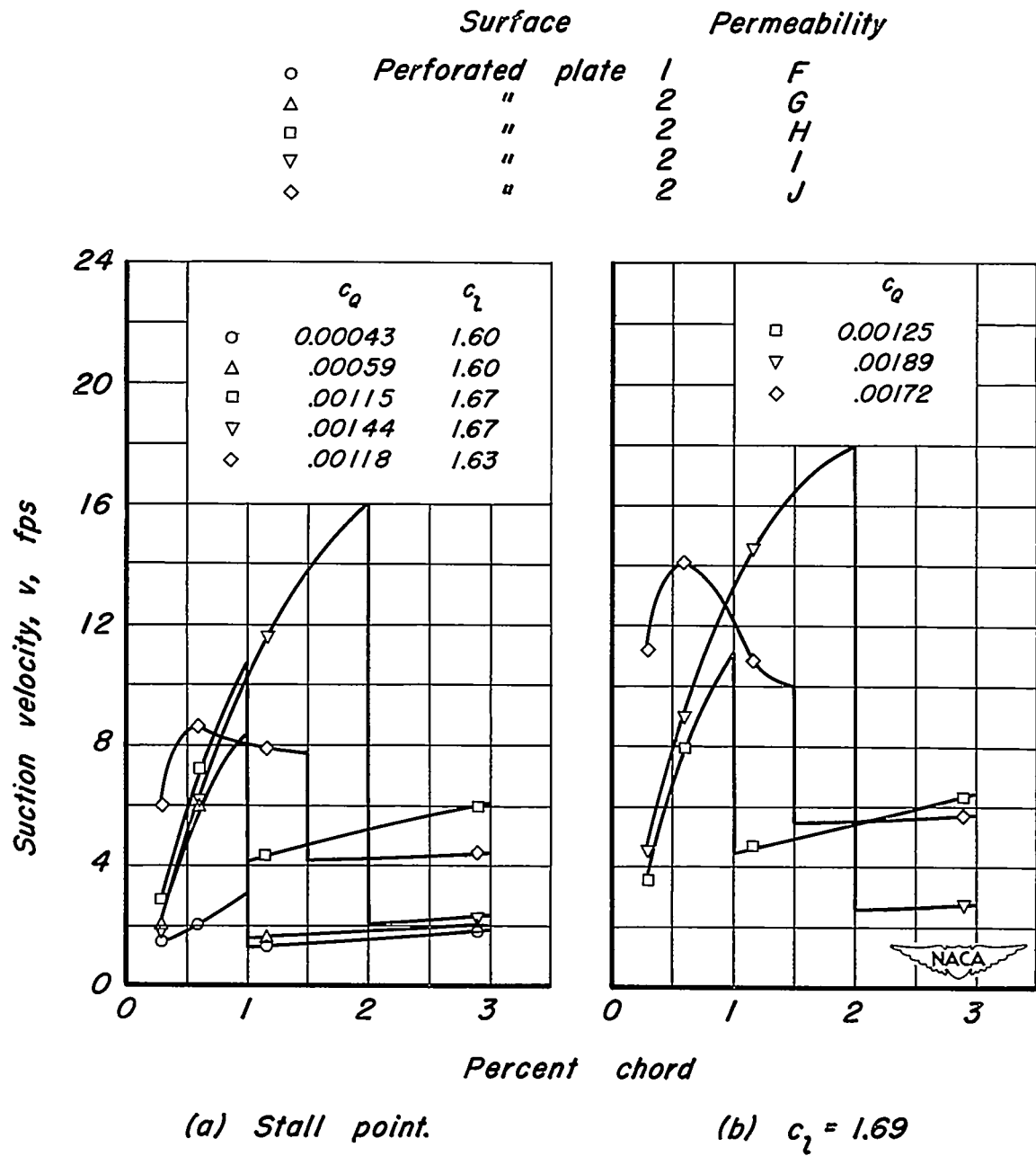
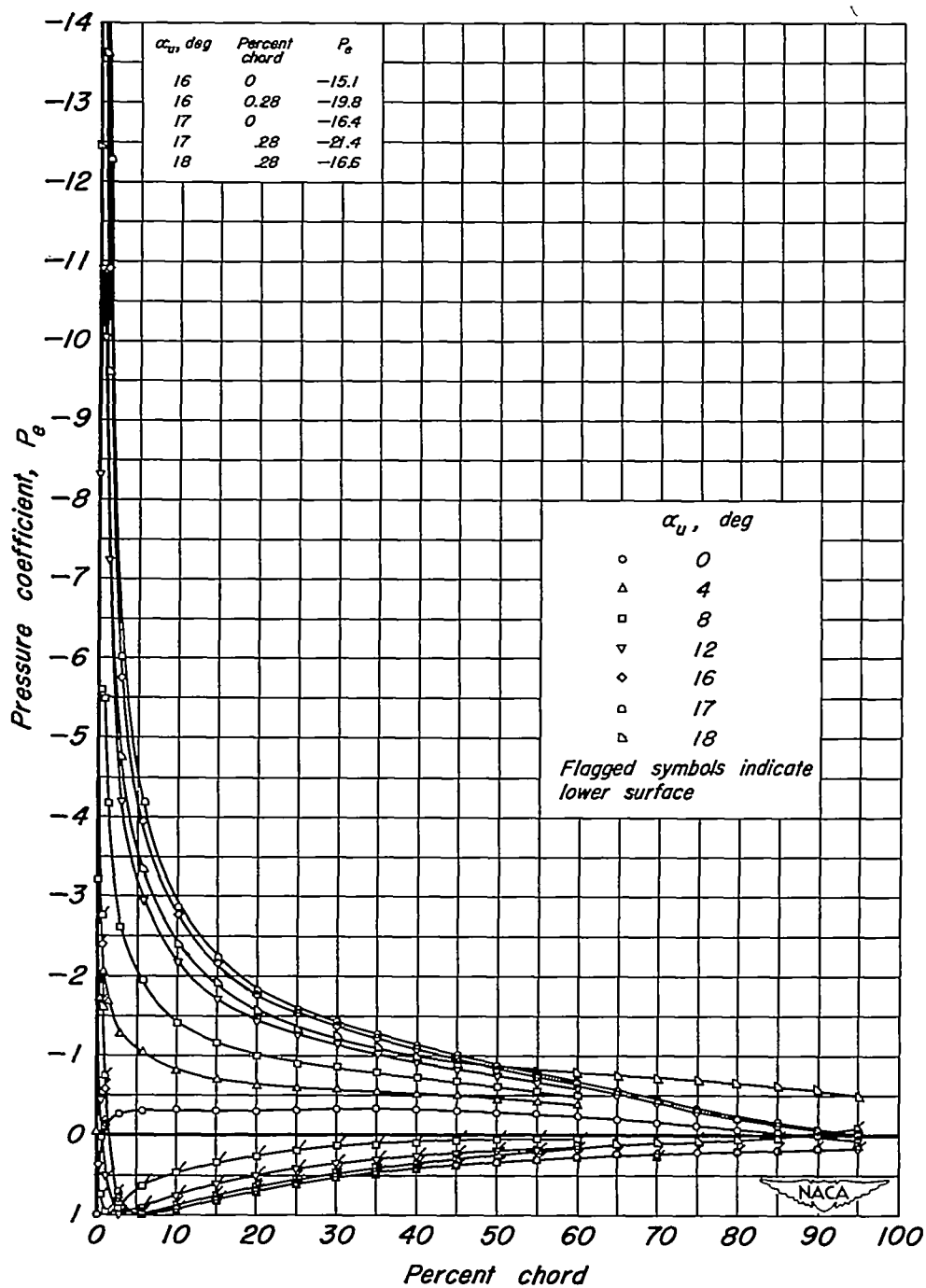
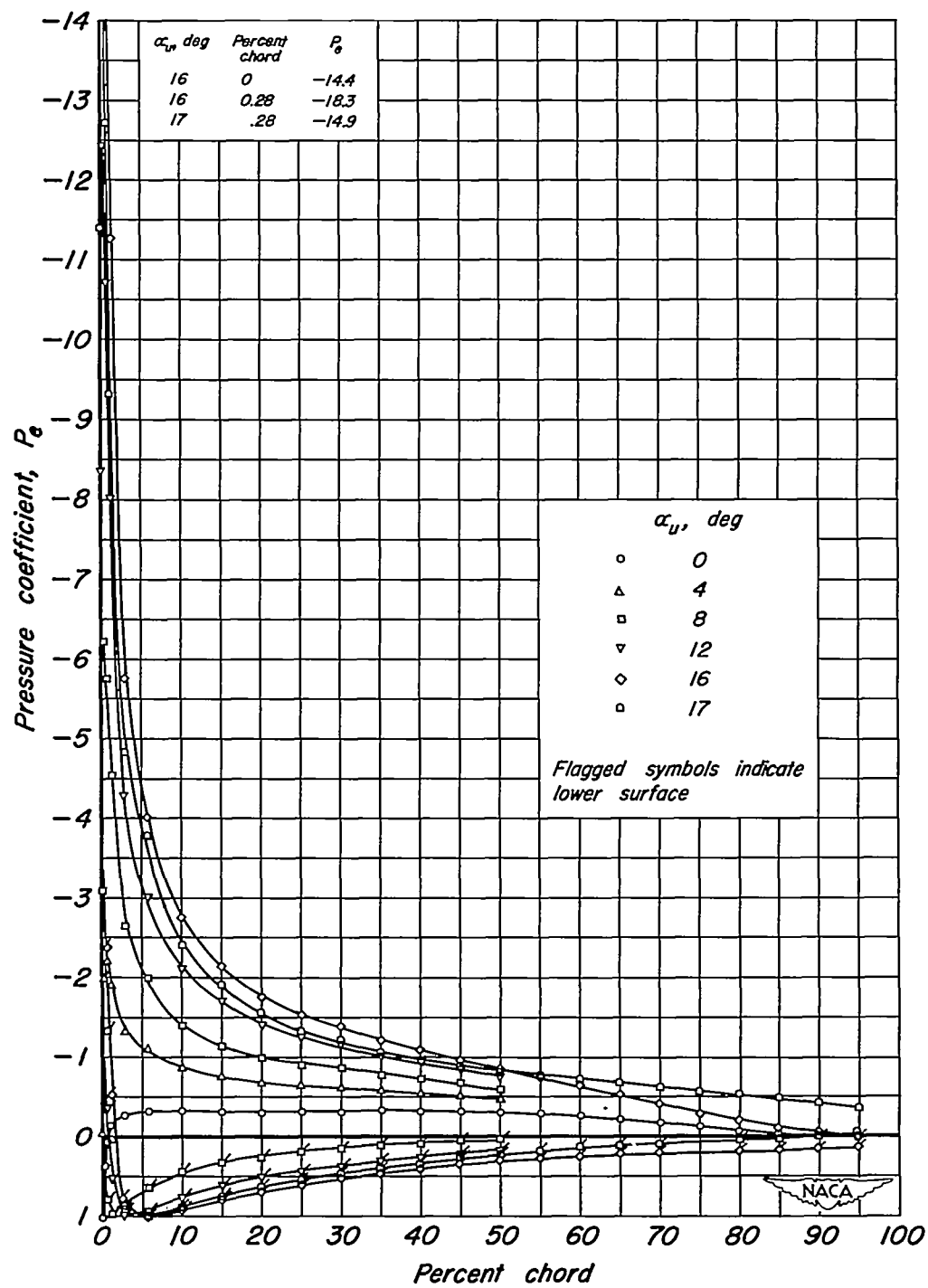


Figure 24.- Stall-point suction velocity distributions for stepped-type permeability arrangements. $\alpha_u = 16^\circ$, $U_o = 162$ fps.



(a) $v_{0.6} = 14$ fps

Figure 25.- Chordwise distribution of pressure over the model with perforated plate I and permeability arrangement G. $U_0 = 162$ fps.



(b) $v_{0.6} = 8$ fps

Figure 25.- Concluded.

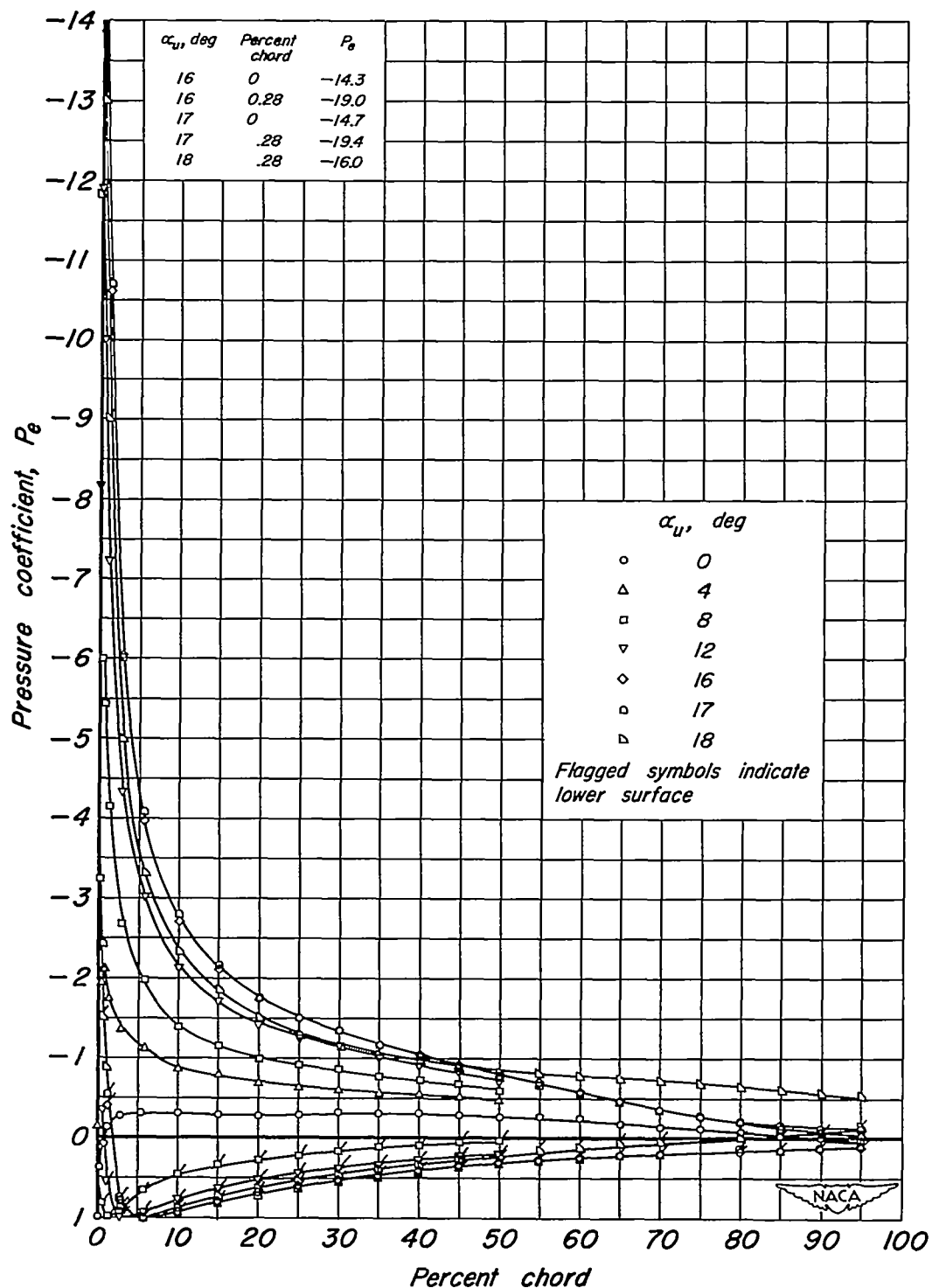


Figure 26.- Chordwise distribution of pressure over the model with perforated plate 2 and permeability arrangement J.
 $v_{\alpha 6} = 16$ fps, $U_o = 162$ fps.

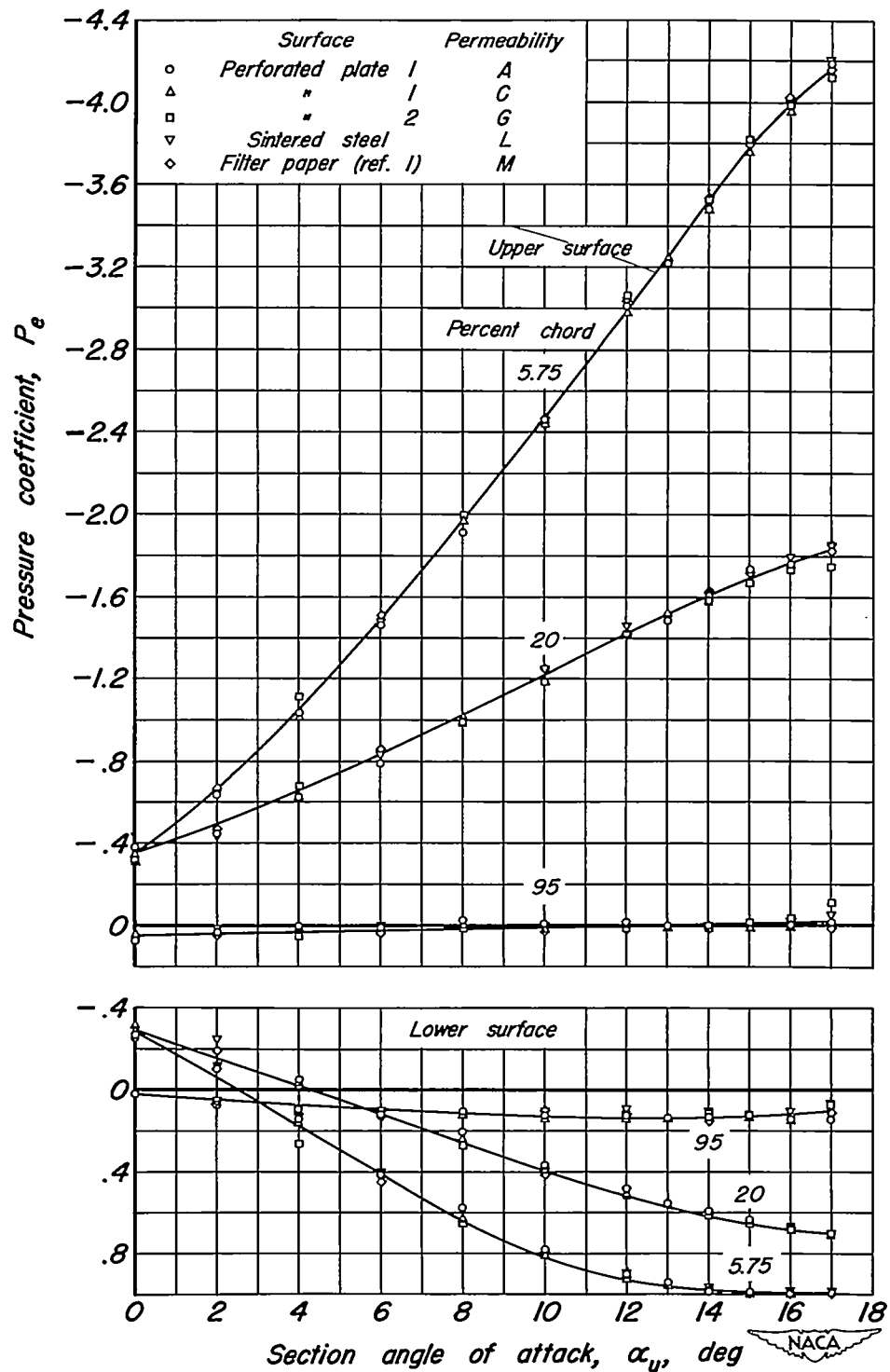


Figure 27.- Variation of the pressure coefficients at particular chordwise stations with angle of attack for various surface materials and permeability arrangements tested. $U_o = 162$ fps.

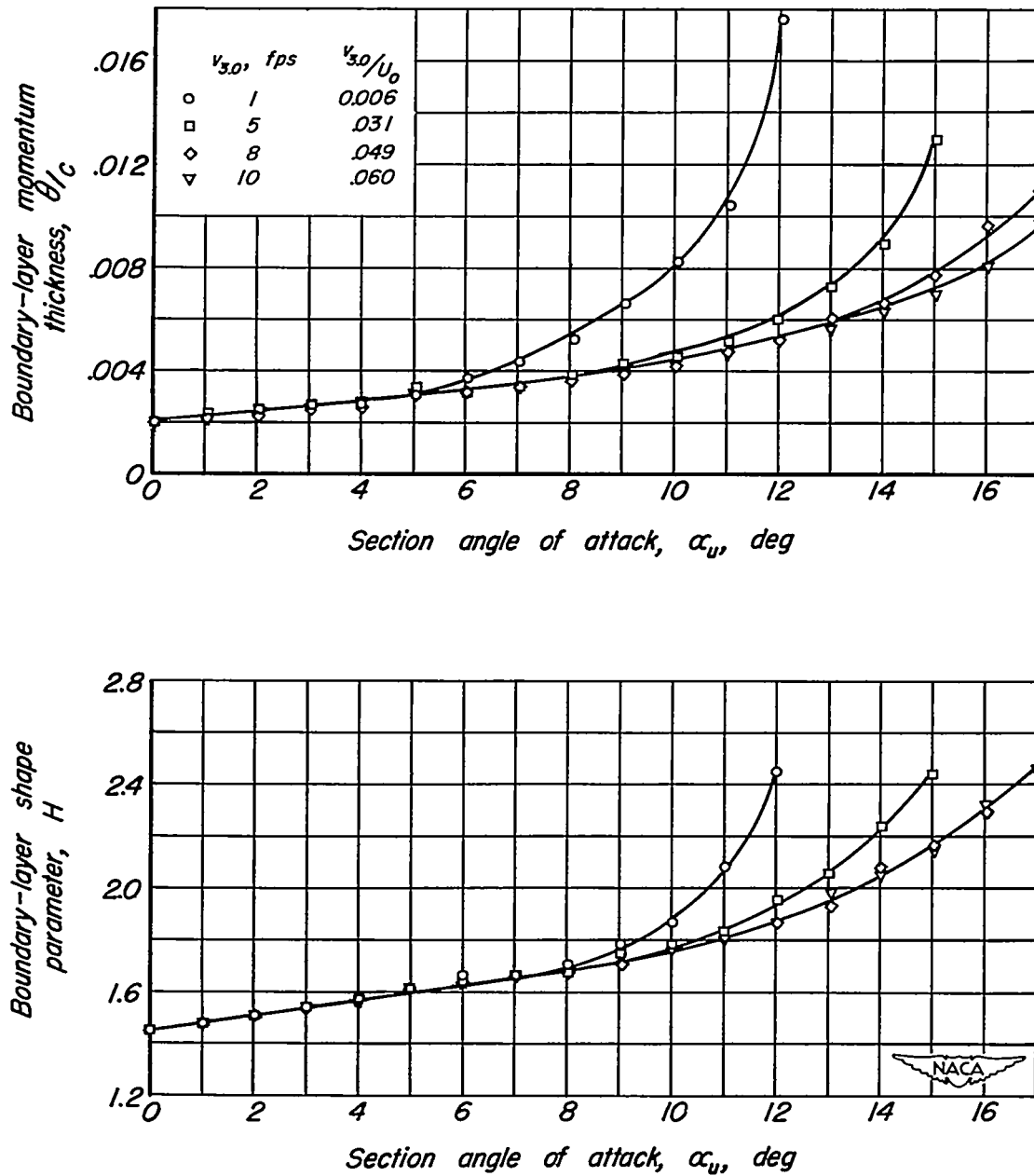


Figure 28.- Boundary-layer parameters at 95-percent chord for the model with sintered steel and permeability arrangement K. $U_0=162$ fps.

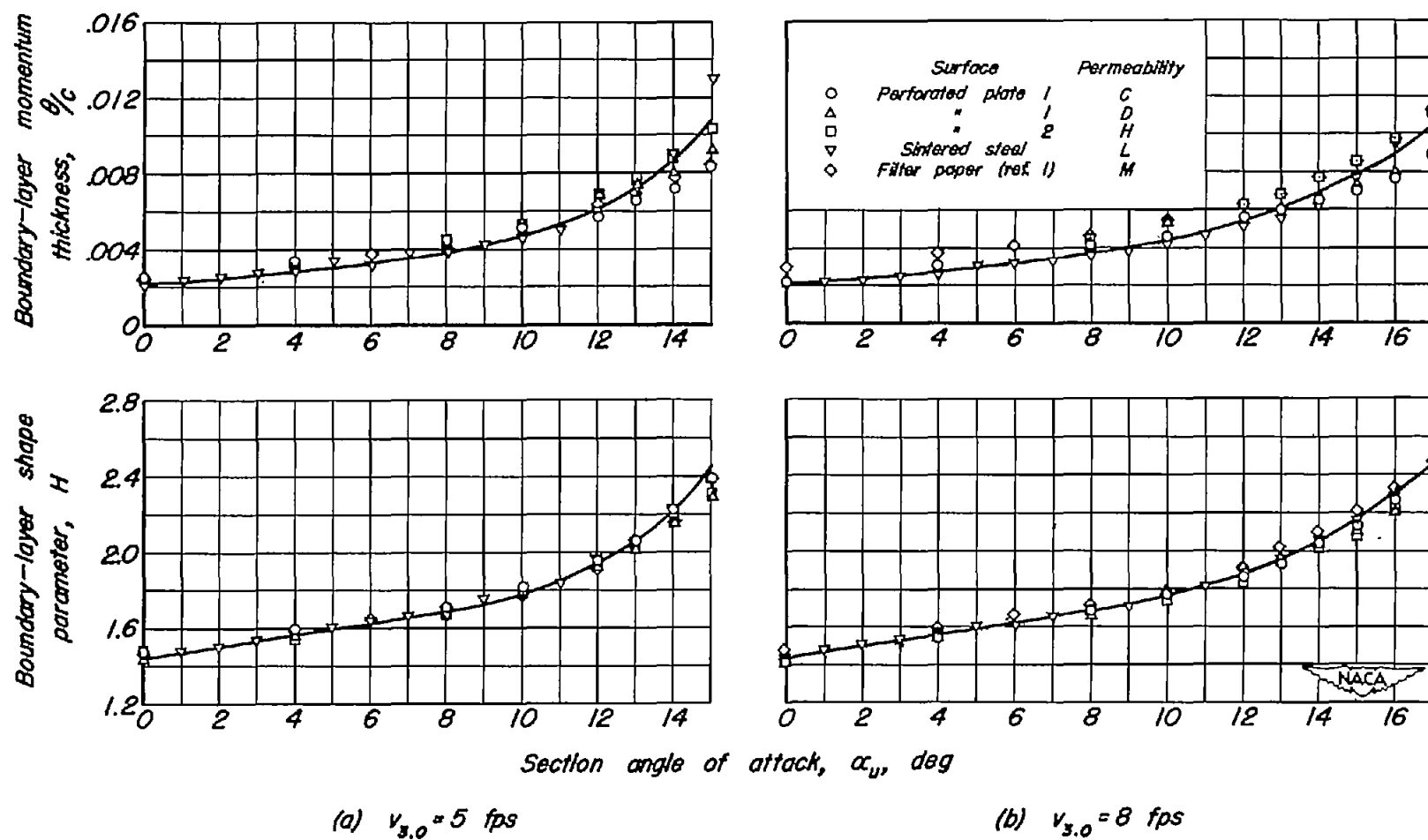
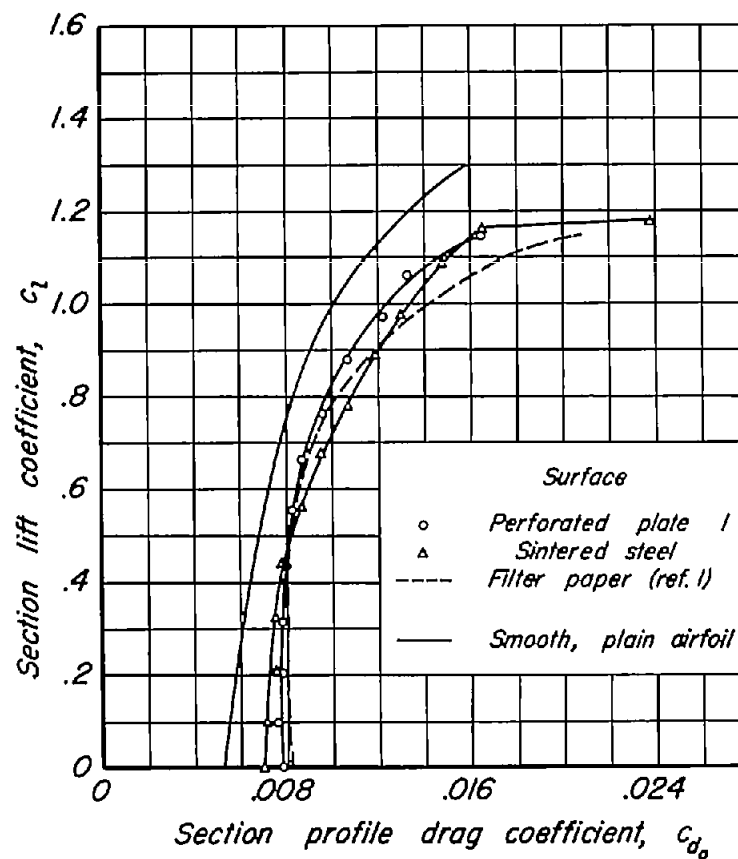
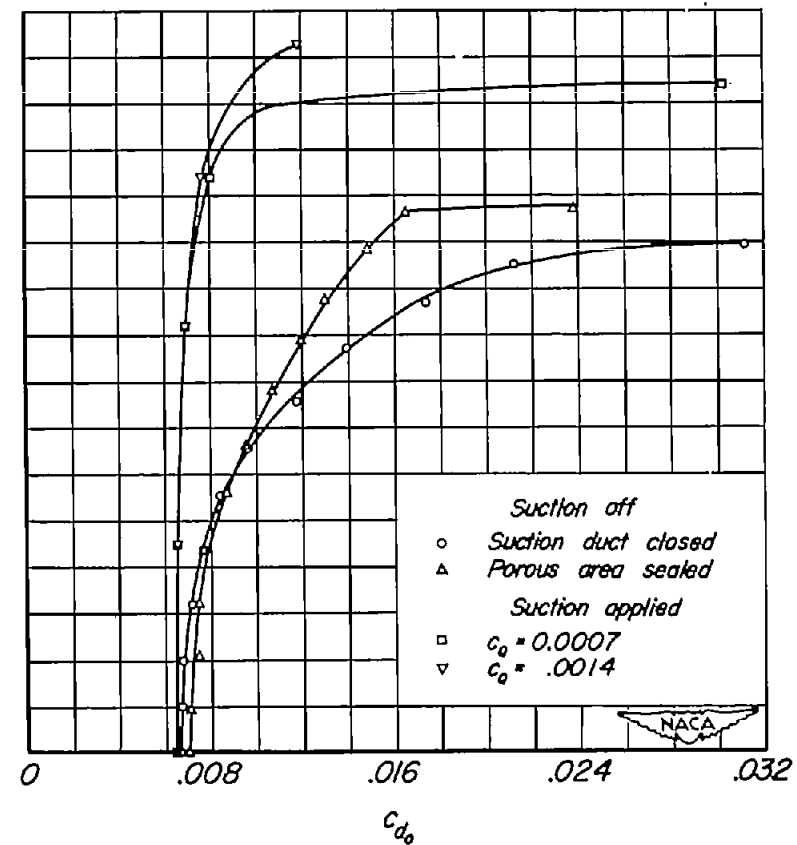


Figure 29. - Variation of the boundary-layer parameters at 95-percent chord with angle of attack for various surface materials and permeability arrangements. $U_\infty = 162$ fps.



(a) Suction off, porous area sealed.



(b) Sintered steel with permeability K .

Figure 30.- Variation of profile drag coefficient with section lift coefficient. $U_0 = 187$ fps.

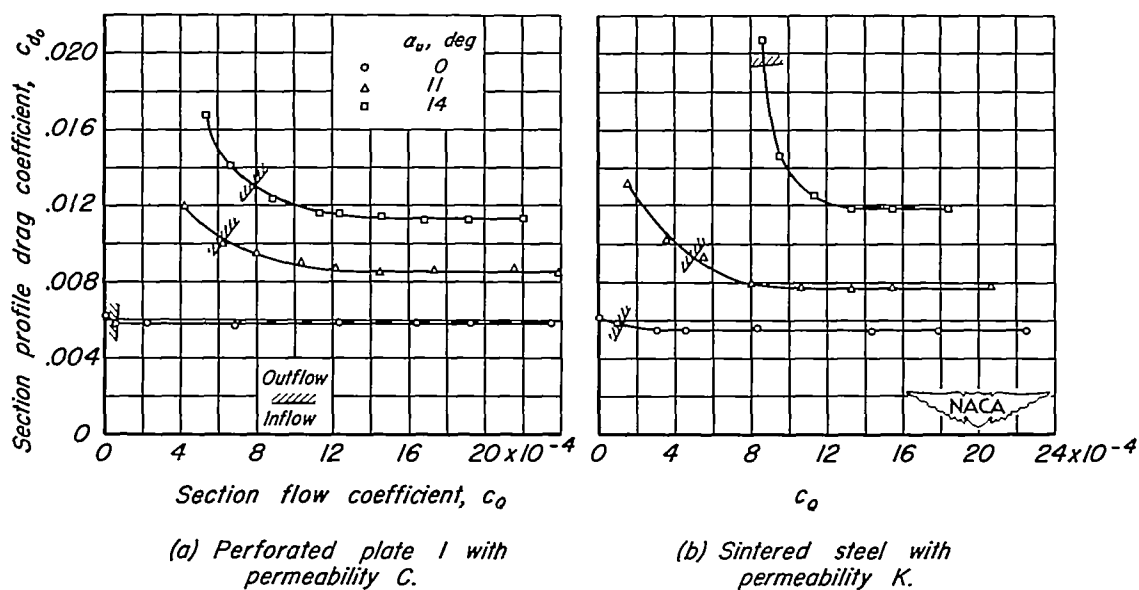


Figure 31. - Variation of profile drag coefficient with section flow coefficient. $U_o = 187$ fps.

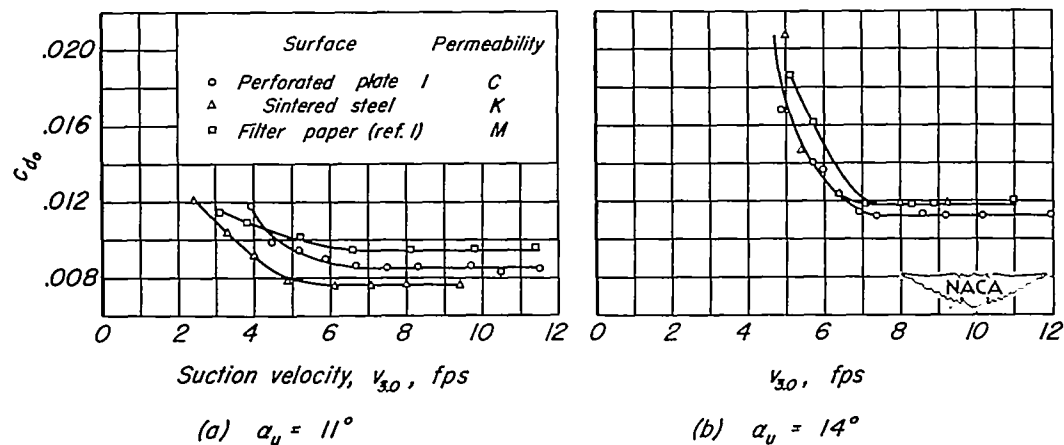


Figure 32. - Variation of profile drag coefficient with suction velocity at trailing edge of suction area. $U_o = 187$ fps.

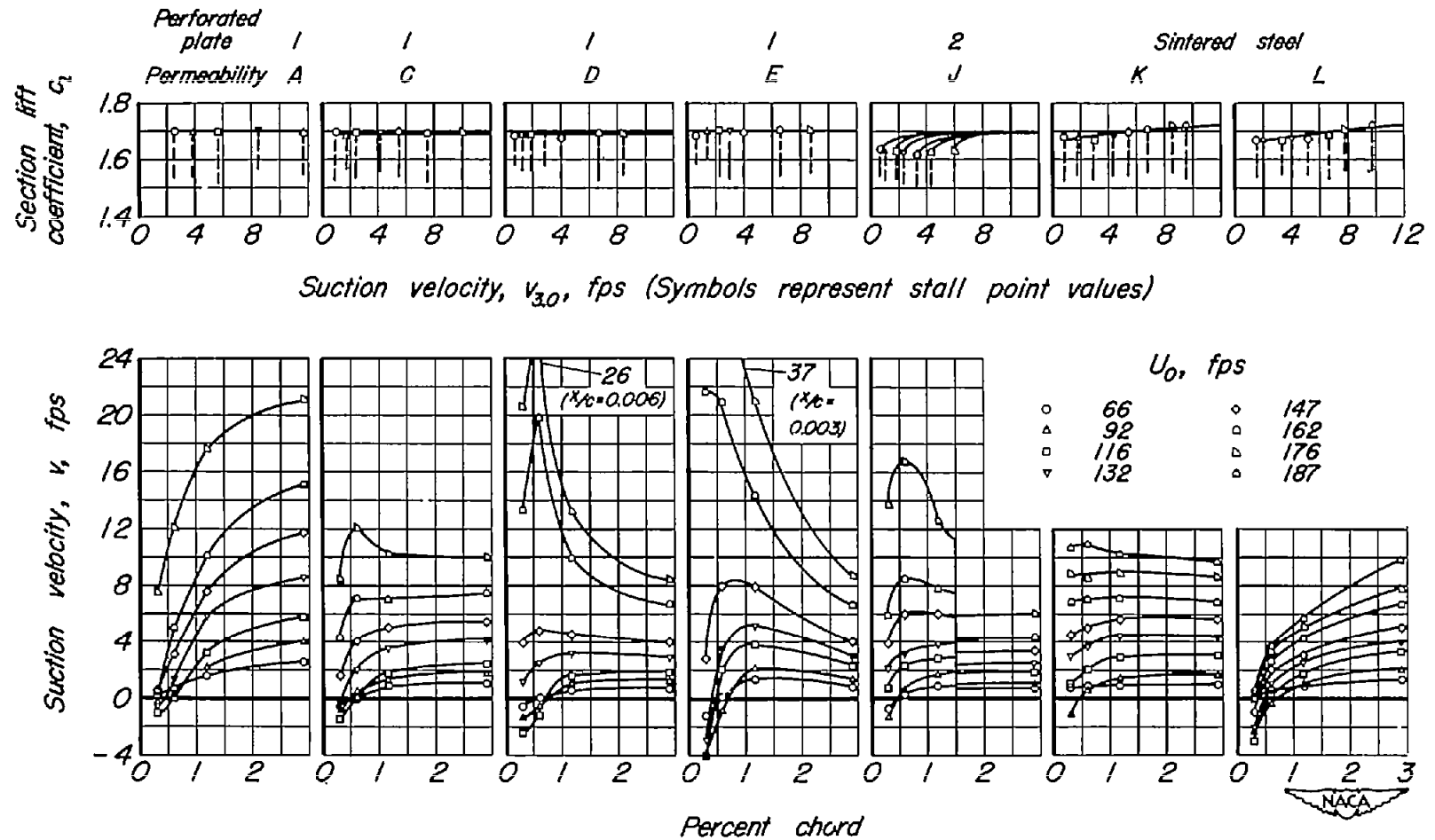


Figure 33.- Effect of free-stream velocity on the stall-point suction velocity distributions for various permeability arrangements. $\alpha_u = 16^\circ$.

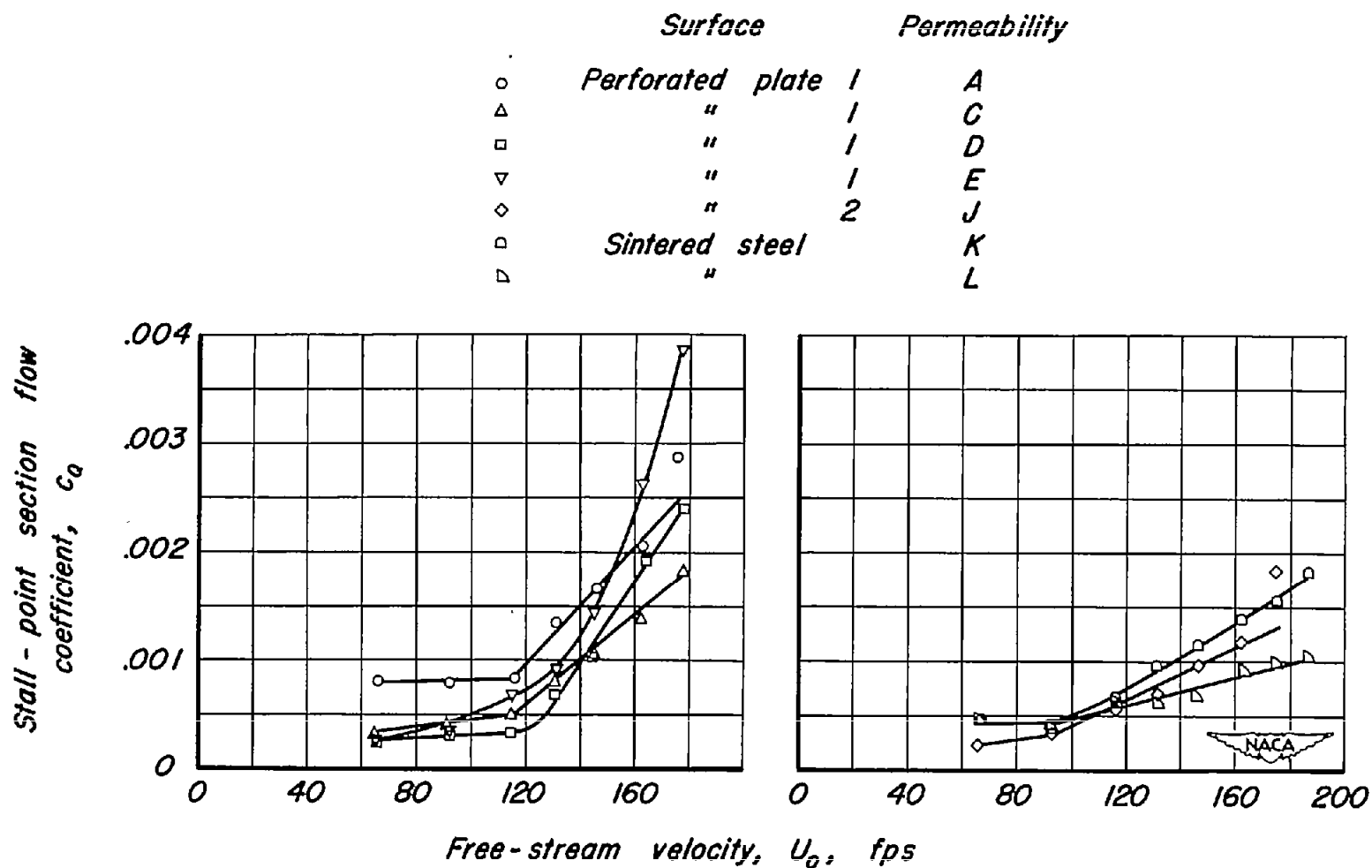


Figure 34.- Variation of stall-point section flow coefficient with free-stream velocity for various permeability arrangements. $\alpha_u = 16^\circ$.

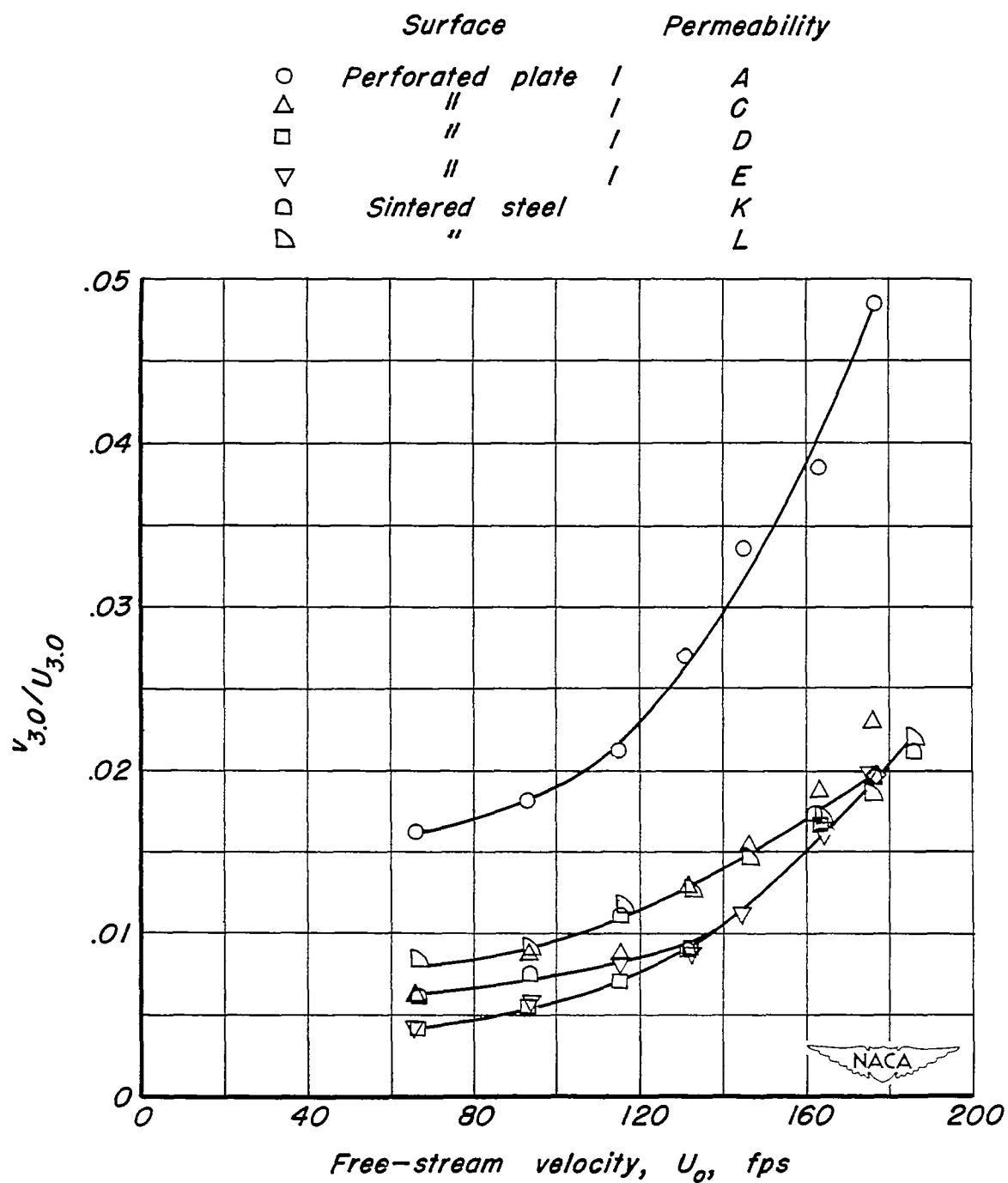


Figure 35.- Variation of the stall-point suction velocity ratio with free-stream velocity for the smooth-type permeability arrangements. $\alpha_u = 16^\circ$.

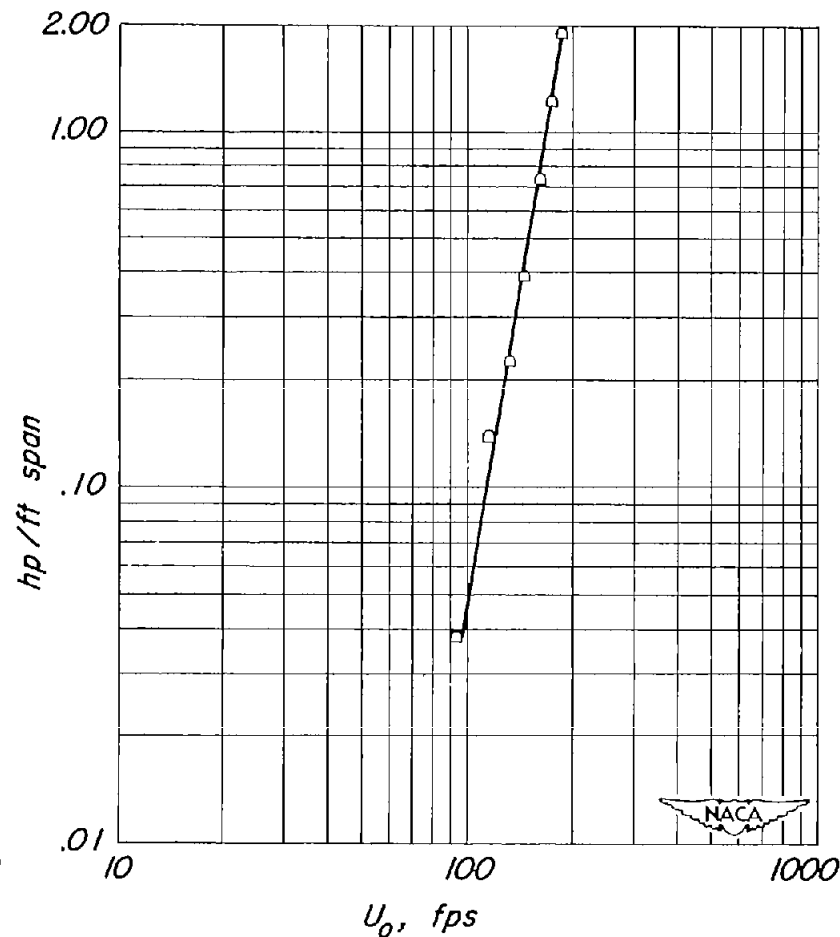
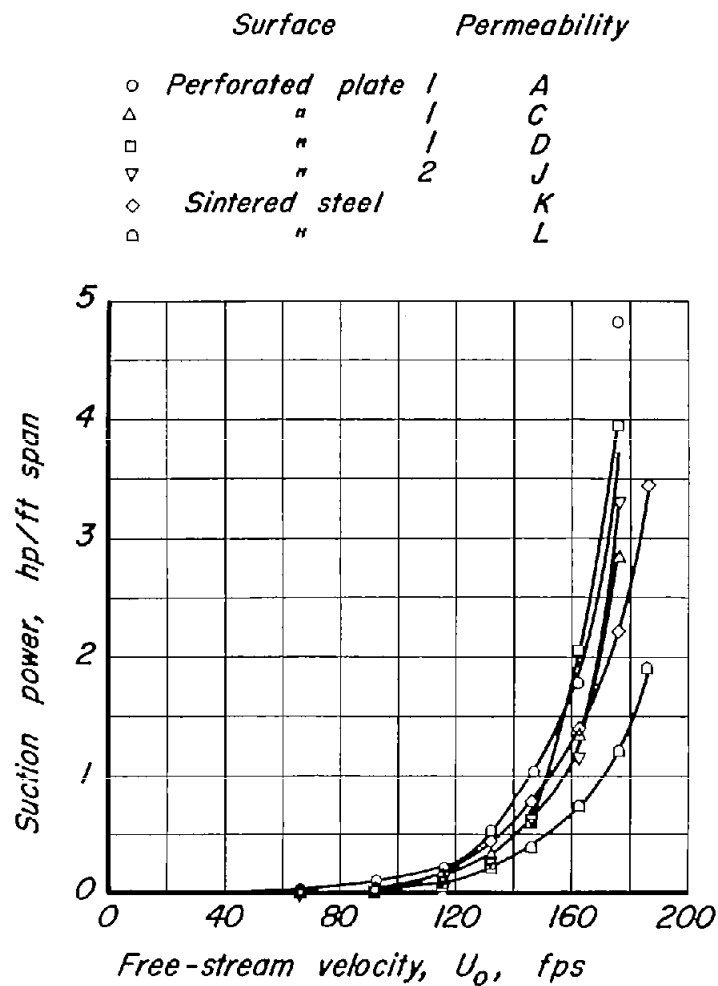


Figure 36.-Variation of the stall-point suction power with free-stream velocity for various permeability arrangements. $\alpha_u = 16^\circ$.